Available online at www.springerlink.com

SpringerLink

Ocean Science Journal

Article

Cochlodinium polykrikoides Red Tide Detection in the South Sea of Korea using Spectral Classification of MODIS Data

Young Baek Son[1,2]*, Joji Ishizaka[2], Jong-Chul Jeong[3], Hyun-Choel Kim[4], and Taehee Lee[5]

[1]*Korea Ocean Satellite Center (KOSC), KORDI, Ansan P.O. Box 29, Seoul 425-600, Korea*
[2]*Hydrospheric Atmospheric Research Center (HyARC), Nagoya University, Furo-cho, Chigusak-ku, Nagoya, Aichi 464-8601, Japan*
[3]*Department of Geoinformatics Engineering, Namseoul University, 21 Maeju-ri, Cheonan 330-800, Korea*
[4]*Korea Polar Research Institute, KORDI, Incheon 406-840, Korea*
[5]*South Sea Environment Research Department, South Sea Branch, KORDI, Geoje 656-830, Korea*

Abstract – To distinguish true red tide water (particularly *Cochlodinium polykrikoides* blooms) from non-red tide water (false satellite high chlorophyll water) in the South Sea of Korea, we developed a systematic classification method using spectral information from MODIS level products and applied it to five different harmful algal bloom events. Red tide and non-red tide waters were classified based on four different criteria. The first step revealed that the radiance peaks of potential red tide water occurred at 555 and 678 nm. The second step separated optically different waters that were influenced by relatively low and high contributions of colored dissolved organic matter (CDOM) (including detritus) to chlorophyll. The third and fourth steps discriminated red tide water from non-red tide water based on the blue-to-green ratio in areas with lower and higher contributions of CDOM to chlorophyll, respectively. After applying the red tide classification (using the four criteria), the spectral response of the red tide water, which is influenced by pigment concentration, showed different slopes for the blue and green bands (lower slope at blue bands and higher slope at green bands). The opposite result was found for non-red tide water, due to decreasing phytoplankton absorption and increasing detritus/CDOM absorption at blue bands. The results were well matched with the discoloration of water (blue to dark red/brown) and delineated the areal coverage of *C. polykrikoides* blooms, revealing the nature of spatial and temporal variations in red tides. This simple spectral classification method led to increase user accuracy for *C. polykrikoides* and non-red tide blooms (>46% and >97%) and provided a more reliable and robust identification of red tides over a wide range of oceanic environments than was possible using chlorophyll *a* concentration, chlorophyll anomaly, fluorescence analysis, or proposed red tide detection algorithms.

1. Introduction

Satellite remote sensing has been successfully employed to monitor the increasing spatial and temporal scales of red tide under various water conditions, as part of monitoring and detecting harmful algal blooms (HABs) (Stumpf et al. 2003; Hu et al. 2004, 2005; Suh et al. 2004; Ahn and Shanmugam 2006; Ahn et al. 2006; Ishizaka et al. 2006). Most efforts to detect and monitor red tides are based on chlorophyll *a* concentrations (Stumpf et al. 2003; Tomlinson et al. 2004, 2009; Hu et al. 2005; Ahn and Shanmugam 2006; Ishizaka et al. 2006). Stumpf et al. (2003) and Tomlinson et al. (2004) use a chlorophyll anomaly calculated from 2 month averaged SeaWiFS chlorophyll *a* concentrations to detect a potential algal bloom from non-bloom water. This method has been officially employed by the NOAA Coastal Watch Program for HAB monitoring off Florida (Stumpf et al. 2003). The blue-to-green ratio algorithm (O'Reilly et al. 2000) provides reasonable estimates of chlorophyll concentrations in Case I Water, in which chlorophyll is the optically dominant constituent; however, the algorithm is not robust in Case II Water, in which colored dissolved organic matter (CDOM) and/or suspended sediment are present. These constituents cause an increase in absorption

Springer

of blue bands and influence the spectral ratio of reflectance (Carder et al. 1999; Sathyendranath et al. 2001; Siegel et al. 2005), resulting in erroneously high estimates of chlorophyll concentrations and mis-identifing as red tide water (Hu et al. 2003; Ahn and Shanmugam 2006).

To reduce the error arising from the influence of CDOM, Hu et al. (2005) introduced modified chlorophyll concentrations using moderate resolution imaging spectroradiometer (MODIS) fluorescence line height (FLH) to detect *Karenia brevis* blooms in western Florida in the presence of abundant CDOM and inorganic particulate matter. The chlorophyll fluorescence band is useful for separating true pigment concentrations from the strong influence of CDOM effects (Letelier and Abbott 1996; Hu et al. 2005); however, the MODIS FLH approach simply uses a radiance peak of 678 nm compared with the bottom line of 667 and 748 nm (Letelier and Abbott 1996; Esaias et al. 1998) and is less sensitive in the case of high concentrations of suspended sediment due to increasing interactions between chlorophyll and suspended sediment (Babin et al. 1996; Ahn and Shanmugam 2006). Furthermore, these bands are not incorporated in the SeaWiFS sensor (Hooker et al. 1994).

Recently, new approaches to monitor red tides have been developed based on optical closure relationships, using semi-analytical and model-based approaches, between reflectance spectra or normalized water-leaving radiance (nLw) and the relevant inherent optical properties (IOPs) of seawater (Dierssen et al. 2006; Cannizzaro et al. 2008; Sasaki et al. 2008). Sasaki et al. (2008) and Dierssen et al. (2006) provided a discernible absorption or reflectance peak during a red tide shift to longer wavelength around 570-590 nm. Backscattering spectra are systematically used to identify *K. brevis* blooms based on low backscattering to high chlorophyll concentration (Cannizzaro et al. 2008). The two most common red-tide species, dinoflagellates and diatoms, have similar absorption characteristics under natural water conditions. The spectral magnitude also changes depending on the species and the concentration of the organism (Ahn and Moon 1998; Schofield et al. 1999; IOCCG 2000; Ahn et al. 2006; Dierssen et al. 2006; Sasaki et al. 2008). Although these empirical and model-based approaches employ full spectral radiance information and are well correlated with a broad range of pigment concentrations, further studies are necessary to establish a data bank of spectral signatures of different water constituents using multispectral, multivariate data (IOCCG 2000).

Red tide events comprising diatom or dinoflagellate blooms within enclosed and semi-enclosed bays of the South Sea of Korea (SSK) have occurred frequently since the early 1990s (Lee et al. 2002). Since 1995, red tides have been dominated by *Cochlodinium polykrikoides* blooms (Kang et al. 2002; Suh et al. 2004; Lee 2006). The duration and areal extent of red tides have been increasing in both inshore and offshore areas of Korean waters, particularly in the SSK and on the east and west coasts of Korea (NFRDI 2004, 2005; Suh et al. 2004; Lee 2006; http://www.nfrdi. re.kr/redtideInfo). *C. polykrikoides* blooms have occurred at frequent intervals in clear, offshore waters between Naro-do and Namhae-do and are then transported to inshore or offshore areas (Fig. 1). Kim et al. (1999) and Lee (2008) suggested that the *C. polykrikoides* blooms around Naro-do are related to frontal mixing between coastal water and warm offshore water (e.g. the Tsushima Warm Current), driven by northeasterly winds. The blooms extend from the east coast at times of strong southwesterly winds (Lee 2008). One of the most important phenomena in this regard is that *C. polykrikoides* blooms are geographically unconstrained, extending from turbid water in the southwest SSK and the Yellow Sea to clear offshore waters (Yoo and Jeong 1999; Suh et al. 2004; Lee 2006). Several recent works (Suh et al. 2004; Ahn and Shanmugam 2006; Ahn et al. 2006; Kim et al. 2009) have greatly expanded our knowledge on many red tide and non-red tide blooms parameters from remote sensing ocean color data and *in-situ* observations to assess increasing spatial and temporal coverage in Korean coastal waters.

However, previously defined studies are enough to significantly expand our understanding of how red tide blooms (HAB) clarify non-red tide water in hydrographically various water conditions. Thus, we used the available information for a continuous and systematic study of algal blooms in this study. The combined analysis using the simple spectral classification and band ratio tested to develop the most accurate detection of algal bloom using MODIS spectral data. The purpose of this study was to (1) identify the spectral characteristics of red tides (specifically *C. polykrikoides* blooms) based on radiance, satellite chlorophyll *a* concentration, and FLH and IOP derived from MODIS ocean color data; (2) distinguish true red tide water from non-red tide water (false satellite high chlorophyll water); (3) map areas of red tide in the SSK; and (4) compare user accuracy of seven

different red tide detection algorithms.

2. Data and Methods

Temporal and spatial information of red tide events from 2002 to 2007 were obtained from the National Fisheries Research and Development Institute of Korea (NFRDI, http://www.nfrdi.re.kr/redtideInfo). NFRDI issues a red tide "attention" or "alert" to fisherman and aqua-farmers when the density of *C. polykrikoides* exceeds 300 cells/ml or 1,000 cells/ml, respectively. We selected five clear ocean color images covering the SSK (34°-35.5°N, 126°-129.5°E; Fig. 1) containing red tide information, with different intensities and spatial coverages of *C. polykrikoides* blooms (NFRDI 2004, 2005; Lim et al. 2008; http://www.nfrdi. re.kr/redtideInfo).

Daily data (level 0) obtained by MODIS Aqua satellite were obtained from the NASA Ocean Biology Processing Group (http://oceancolor.gsfc.nasa.gov/) for August 19, 2002, September 8, 2002, August 22, 2003, August 28, 2004, and August 21, 2007. The level 0 data were then processed to L1A and L1B (Franz 2006a). Three visible bands (red: 645 nm; green: 555 nm; blue: 469 nm) from L1B water-leaving radiance data were used to create composite true-color images that optionally provided a partial atmospheric correction to remove the effects of Rayleigh and diffuse transmittance without processing standard mapping (Franz 2006a). The true color images (using three bands) provided greater spatial variability detail than can be obtained from chlorophyll (using two bands) or single wave-band imaging (Hu et al. 2005).

The normalized water-leaving radiance, *nLw*, was estimated by SeaDAS MSL12 (McClain et al. 2004; Franz 2006b), processed using a standard correction algorithm (~1 km resolution) for seven visible bands (412, 443, 488, 531, 555, 667, and 678 nm) and two near-infrared bands (748 and 869 nm) for atmospheric correction (Gordon and Wang 1994). The derived radiance spectra were used for spectral classification, FLH calculation (Letelier and Abbott 1996; Esaias et al. 1998), and chlorophyll *a* concentration (O'Reilly et al. 2000). The satellite-based absorption and scattering coefficients were obtained using the semi-analytical algorithm developed by Carder et al. (1999). Each absorption and backscattering term was separated as $a(\lambda)= a_w(\lambda)+a_{ph}(\lambda)+a_{dg}(\lambda)$ and $b_b(\lambda)=b_w(\lambda)+b_{bp}(\lambda)$, respectively, where a, a_w, a_{ph}, and a_{dg} are the total, water, phytoplankton, and detritus/CDOM absorption coefficients, respectively, and b_b, b_w, and b_{bp} are the total, water, and particle backscattering coefficients, respectively, as a function of wavelength. Each pixel derived from level 2 processes included information on chlorophyll *a* concentration, FLH, multi-spectra of nLw, a_{ph}, a_{dg}, and b_{bp}.
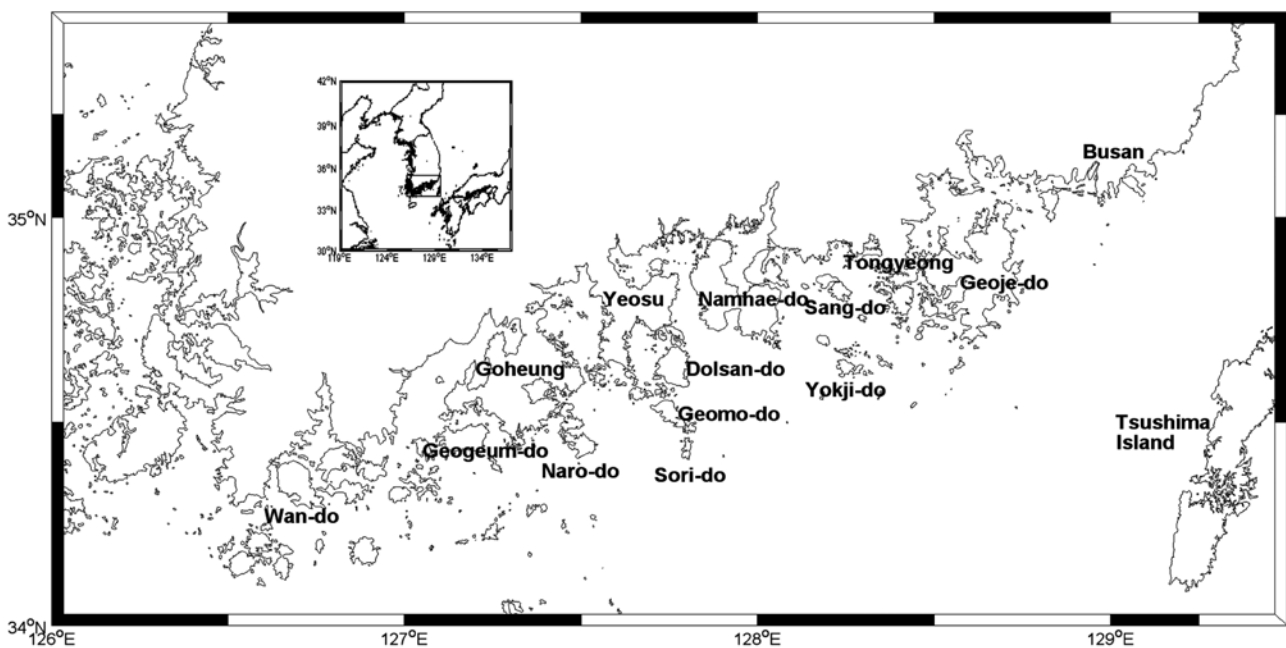

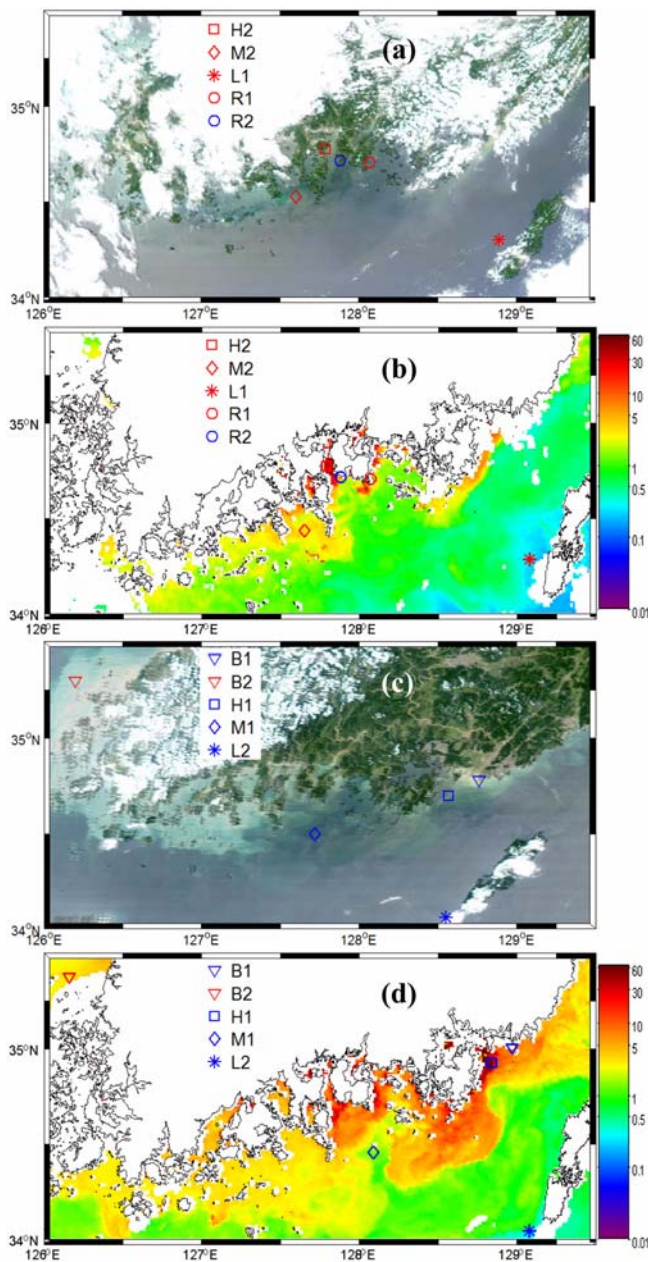**Fig. 1.** Map of the South Sea of Korea (SSK)

Fig. 2. A true color image on August 19, 2002 (a) and September 8, 2002 (c) generated from 645 nm (red), 555 nm (green), and 469 nm (blue) water-leaving radiance. Daily MODIS standard chlorophyll-a concentration (mg/m^3) on August 19, 2002 (b) and September 8, 2002 (d). Sub-sample location is denoted with bright color, high, moderate, low satellite chlorophyll, and red tide area (B, H, M, L, and R)

To assess the spectral characteristics of different water masses, 10 sub-areas were selected from areas with bright color, high satellite chlorophyll (>5 mg/m^3), moderate satellite chlorophyll (1-5 mg/m^3), low satellite chlorophyll (<0.1 mg/m^3), and red tide on August 19, and September 8, 2002

(Fig. 2). Each MODIS-derived sub-sample parameter was averaged from the 3×3 matrix pixel. The selected pixel data (nLw, a_{ph}, a_{dg}, and b_{bp}) were used to determine the optical characteristics of various water conditions ranging from turbid water to clear, open-ocean water.

To quantify the different spectral responses of true red tide and false satellite high chlorophyll water, ~600 pixel data (nLw, chlorophyll a concentration, FLH, a_{ph}, a_{dg}, and b_{bp}) were also selected from five different satellite images. The sub-sample areas of high satellite chlorophyll were chosen from water with high chlorophyll concentration (>3 mg/m^3). Red tide sub-samples were collected from areas identified on NFRDI red-tide maps (NFRDI 2004, 2005; Lim et al. 2008; http://www.nfrdi.re.kr/redtideInfo). Radiance band ratios were used to determine the red tide and non-red tide conditions, combined with the results of chlorophyll, FLH, and IOP analyses. In this study, red tide was defined as a *C. polykrikoides* bloom and non-red tide as the clear water and/or the water of the increased satellite chlorophyll concentration without harmful algal (*C. polykrikoides*) bloom.

Using the spectral classification method and ocean color data, we demonstrated how the proposed method improves the detection of the spatial and temporal distribution of *C. polykrikoides* blooms using a simple classification scheme.

Finally, we calculated and compared the accuracy of six different red tide detection algorithms (Table 1) and our analysis. In Table 1, chlorophyll anomaly, b_{bp}/b_{bp}_morel, FLH, and SS algorithms were developed for detecting *K. brevis* blooms in the Gulf of Mexico and TSF and FRTD approaches for *C. polykrikoides* blooms in the SSK. All analyses in this study were processed based on MODIS data. The accuracy of six different red tide detection algorithms and our analysis was estimated based on the relationship between satellite and reference data (Table 2; Kim et al. 2009; Tomlinson et al. 2009) as:

Total accuracy (%) = [(TP + TN)/(TP + FN + FP + TN)] × 100
Precision (%) = [TP/(TP + FP)] × 100
User Accuracy for *C. polykrikoides* bloom = [TP/(TP + FN)] × 100
User Accuracy for non-red tide = [1- {FP/(FP + TN)}] × 100

where TP, FN, FP, and TN are true positive, false negative, false positive, and true negative, respectively.

Table 1. Summary of six different red tide detection methods

Method	Description
Chlorophyll Anomaly (Stumpf et al. 2003; Tomlinson et al. 2004, 2009)	Defined as the difference in satellite chlorophyll values between a single image and a 60-day running mean, ending 2 weeks prior to the image. When satellite chlorophyll anomaly is over 1 mg/m^3, it considers *K. brevis* bloom. (where satellite chlorophyll is MODIS standard chlorophyll in this study).
b_{bp}/ b_{bp}_morel (Morel 1988; Carder et al. 1999; Canizzaro et al. 2008; Tomlinson et al. 2009)	$b_{bp}(555)$ = -0.00182 + 2.058 × Rrs(555) $b_{bp}(555)$_Morel = 0.3(chl)$^{0.62}$ × {0.002+0.02 × [0.5-0.25 × $\log_{10}$(chl)]} $b_{bp}(555)$/ $b_{bp}(555)$_Morel is used to indicate *K. brevis* bloom, when the value is 2 or less. (where chl is MODIS standard chlorophyll in this study).
Fluorescence line height (**FLH**) (Hu et al. 2005)	MODIS FLH is used to indicate *K. brevis* bloom, when the value is above 0.12 mw/cm^2/μm/sr. (In this study, the threshold is used for above 0.10 mw/cm^2/μm/sr).
Spectral Shape at 490 nm (**SS**) (Wynne et al. 2008; Tomlinson et al. 2009)	SS(490) = nLw(488)-nLw(443)-(nLw(531)-nLw(443)) × (488-443)/(531-443) A negative SS(490) was indicative of a *K. brevis* bloom. (Original wavebands for SeaWiFS (443, 490, 510 nm) are modified by MODIS wavelengths (443, 488, 531 nm)).
Two-stage filtering (**TSF**) (Kim et al. 2009)	Step. 1: MODIS sea surface temperature ranged from 22.0-26.0 °C is used for potential red tide area and remove other pixels. Step. 2 : MRI = (nLw(555)-nLw(488))/(nLw(555)+nLw(488)). Positive MRI is potential red tide pixel and negative MRI is clear and/or turbidity water pixel (remove negative MRI pixel). Step. 3 : Remove turbidity water using the threshold of above 1.5 of nLw(667). Step. 4 : Determine the *Cochlodinium polykrikoides* bloom area using local Moran's I spatial statistical method.
Feasibility of red tide detection (**FRTD**) (Suh et al. 2004)	Suspended solid considering particles of red tide bloom = -11.51 × Ln((nLw(488)/nLw(555)) + 14.38 (In this study, original wavebands for SeaWiFS (490 nm) are modified by MODIS wavelengths (488 nm). The threshold used above 15 as *Cochlodinium polykrikoides* bloom.)

Table 2. Accuracy assessments between satellite and reference data (Kim et al. 2009)

		Satellite data	
		Detection *C. polykrikoides* pixels	Detection non-red tide pixels
Reference data	in-situ *C. polykrikoides* pixels	True Positive (TP)	False Negative (FN)
	in-situ non-red tide pixels	False Positive (FP)	True Negative (TN)

3. Results

Spectral characteristics of the water mass

Figure 3 shows the spectral characteristics of $nLw(\lambda)$, $a_{ph}(\lambda)$, $a_{dg}(\lambda)$, and $b_{bp}(\lambda)$ for various water masses. In Figs. 2 and 3a, areas B1 and B2 were defined by the spectra of visually bright brown/yellow areas in the true color composite. Peaks occurred at 531 and 555 nm, with significantly higher radiance values in all green-to-red bands as well as near-infrared. H and R (high satellite chlorophyll concentration and red tide, respectively) areas showed radiance peaks at 555 and 678 nm. A peak at 678 nm, sun-induced chlorophyll fluorescence, was not seen in areas B1 and B2 but was present in areas M1 and M2. For M and L (moderate and low satellite chlorophyll concentration, respectively) areas, the radiance peaks varied from 412 to 531 nm. In Fig. 3b, $a_{ph}(443)$ in areas B1 and B2 was slightly higher than that in area L; the value in areas H was several orders of magnitude higher than that in most other areas (B, M, and L). In Fig.

3c, $a_{dg}(412)$ was higher in areas B, H, and R than in areas M and L. In Fig. 3d, $b_{bp}(555)$ in areas B1 and B2 was several orders of magnitude greater than that in areas H, R, M, and L.

$nLw(555)$ in areas B1 and B2 was 3-4 times greater than that in areas H and R, and was ~8 times greater than that in areas L1 and L2 (Fig. 3a). nLw is generally proportional to backscattering and inversely proportional to absorption (Carder et al. 1999). Increased nLw values were related to increased particle backscattering, and the contributions of phytoplankton to radiance were minimal in all visual bands, which appeared as yellow and brown. H and R areas were strongly influenced by a_{ph} and a_{dg} (Fig. 3b, c), resulting in decreased nLw at blue wavelengths. The H and R areas had similar nLw values as well as similar absorption and backscattering characteristics. Offshore waters with low chlorophyll concentration (L) were less strongly influenced by a_{ph}, a_{dg}, and b_{bp} (Fig. 3b-d). No peak at near-infrared wavelengths accounted for increasing water absorption with negligible scattering. This area was typically characterized
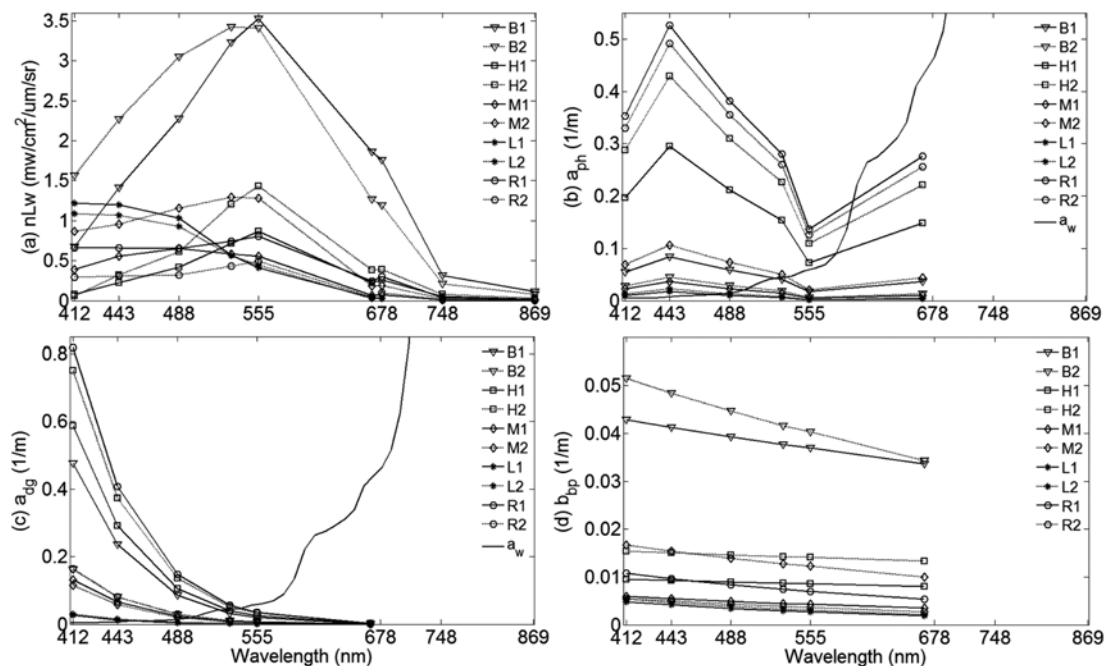
Fig. 3. (a) $nLw(\lambda)$, (b) $a_{ph}(\lambda)$, (c) $a_{dg}(\lambda)$, and (d) $b_{bp}(\lambda)$ versus MODIS wavelengths for 10 different sub-samples, with the aim of determining the spectral characteristics of various water masses. B, H, M, L, and R indicate areas with bright color, high/moderate/low chlorophyll, and red tide, respectively

as less of a contributor of organic/inorganic and dissolved components. The transition areas, M1 and M2, had slightly higher a_{ph}, a_{dg}, and b_{bp} values than did areas L1 and L2 (Fig. 3b-d).

The red tide and high satellite chlorophyll waters in SSK

Based on the results shown in Fig. 3, the H/R and B/M/L areas were distinguished based on contrasting magnitudes of nLw, absorption, and backscattering. The B areas showed a radiance peak in the green band and were strongly influenced by particle backscattering, whereas the H and R areas showed radiance peaks in the green and red bands and were strongly influenced by a_{ph} and a_{dg}. As shown in Fig. 3, the satellite-derived signals in the H and R areas were similar because their spectral characteristics were synchronously determined without any optical differences (Ahn et al. 2006; Dierssen et al. 2006; Sasaki et al. 2008). In an attempt to optically distinguish red tide water from high satellite chlorophyll water, ~600 red tide and high satellite chlorophyll sub-areas collected from five different images were analyzed.

Figure 4 shows the potential red tide spectral curves (left) and high satellite chlorophyll (right) areas averaged over regions with five different satellite chlorophyll concentration

bin values. Both radiance curves (Fig. 4a, b) show two specific spectral characteristics: (1) radiance peaks occur at 555 and 678 nm, and (2) the radiance curves could be distinguished between lower satellite chlorophyll water (LSCW; <10 mg/m^3) and higher satellite chlorophyll water (HSCW; ≥10 mg/m^3). LSCW corresponded to relatively low a_{ph} and a_{dg}, and relatively high b_{bp} in the blue bands (Fig. 4a-h). The radiance signal in HSCW diminished steeply from the green to blue bands, and had relatively higher a_{ph} and a_{dg} values in all visible bands (Fig. 4a-h). The nLw (443) value of LSCW varied from 0.4 to 0.6 mw/cm^2/μm/sr, and that of HSCW varied from 0.2 to 0.3 mw/cm^2/μm/sr. Both radiance values at 443 nm indicated the strong influence of optically different absorption and backscattering, particularly a_{dg}. The slope of both LSCW and HSCW was different; LSCW was less strongly absorbed, whereas HSCW was more strongly absorbed by particulates and dissolved components (Fig. 4i, j).

To optically distinguish between the LSCW and HSCW spectral characteristics, the relationship between the radiance ratio of $nLw(412)$ to $nLw(555)$ and that of ($nLw(555)$ - $nLw(488)$) to $nLw(555)$ was tested (Fig. 5a, b). The radiance ratio of $nLw(412)$ to $nLw(555)$ was negatively co-varied with $a_{dg}(\lambda)$, even though scattering was slightly increased at
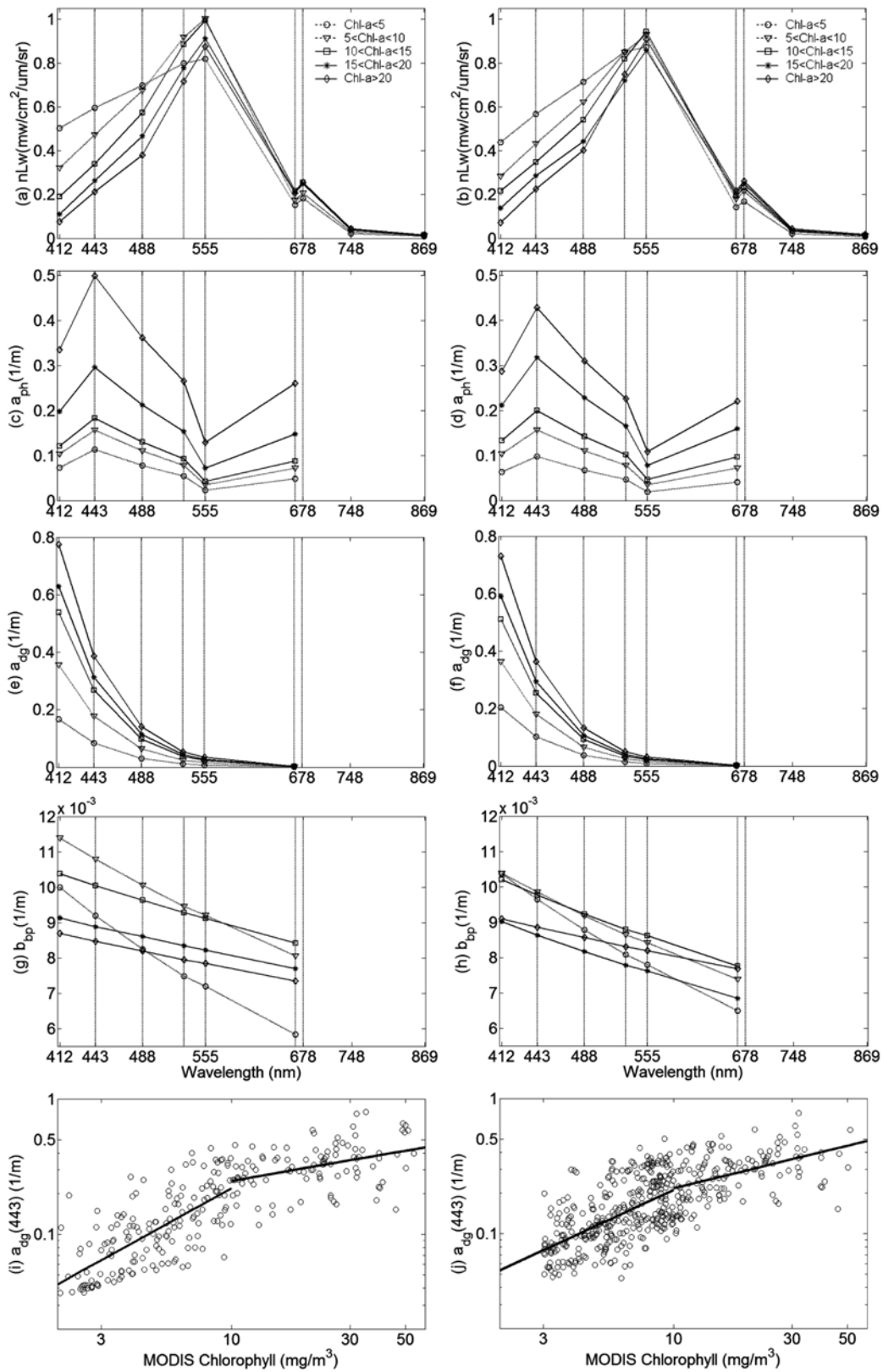
Fig. 4. Red tide (left) and high satellite chlorophyll (right) waters, (a) $nLw(\lambda)$, (b) $a_{\mathrm{ph}}(\lambda)$, (c) $a_{\mathrm{dg}}(\lambda)$, and (d) $b_{\mathrm{bp}}(\lambda)$ are averaged for water with five different bins of chlorophyll concentrations and plotted as a function of wavelength. (i, j) $a_{\mathrm{dg}}(443)$ is plotted with chlorophyll concentrations that show different correlations between >10 and <10 mg/m^3 satellite chlorophyll concentrations
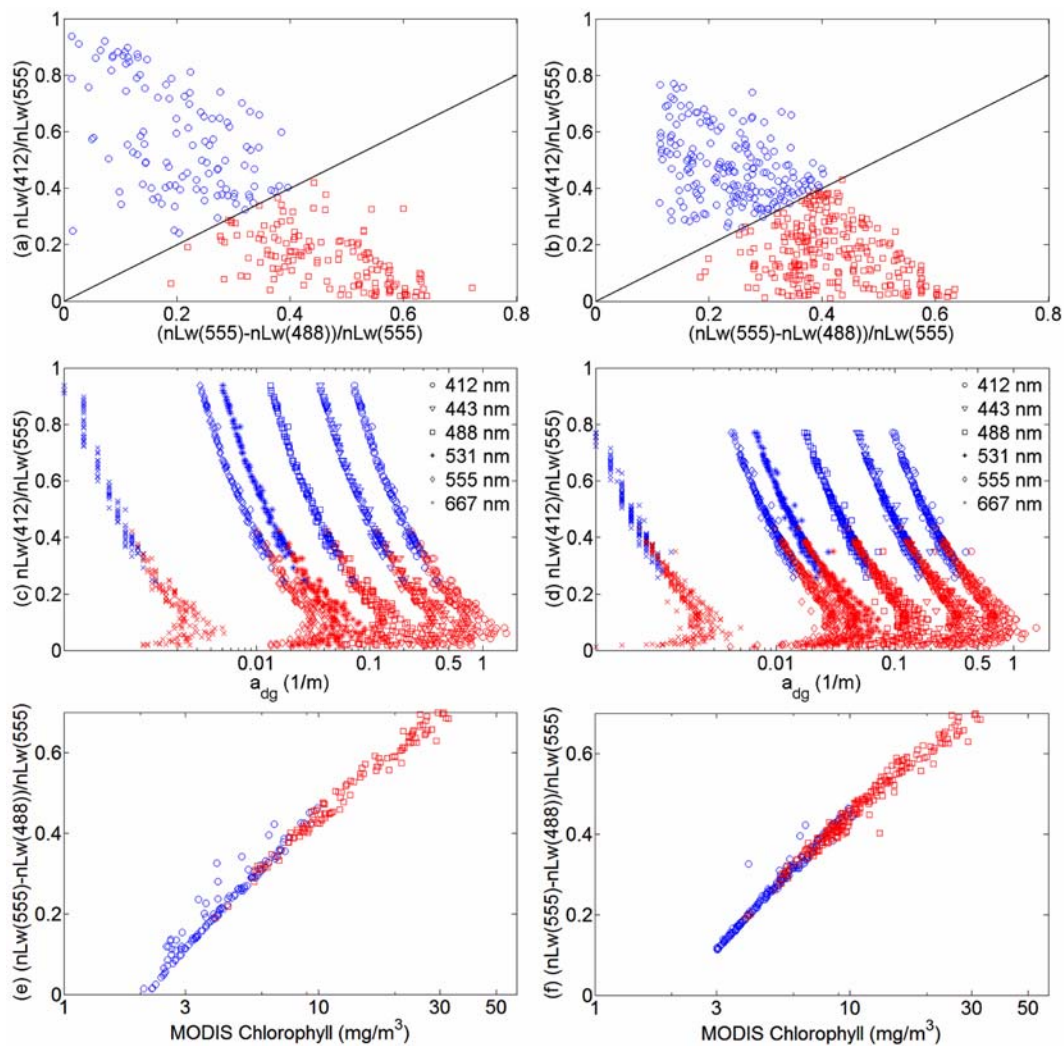
Fig. 5. Blue color shows *nLw*(412)/*nLw*(555) > (*nLw*(555) - *nLw* (488))/*nLw*(555) and red color shows the reverse relationship (a and b) for red tide (left) and high satellite chlorophyll (right) waters. The radiance ratio of *nLw*(412) to *nLw*(555) is plotted as a function of $a_{dg}(\lambda)$ (b and c), and (*nLw*(555) - *nLw*(488))/*nLw*(555) is plotted as a function of chlorophyll concentration (e and f). The relations were used to discriminate optically different waters based on the relative contribution of CDOM (detritus) to satellite chlorophyll

lower values of the ratio (Fig. 5c, d). The radiance ratio of (*nLw*(555) - *nLw*(488)) to *nLw*(555) was positively correlated with satellite chlorophyll concentration (Fig. 5e, f); however, re-plotting the data (e.g. as functions of *nLw*(λ), $a_{ph}(\lambda)$, $a_{dg}(\lambda)$, and $b_{bp}(\lambda)$) using both radiance ratios gave results consistent with those in Fig. 4a-h. To determine the different optical conditions between LSCW and HSCW, the next section tested the condition in which the radiance ratio of *nLw*(412) to *nLw*(555) was greater than that of (*nLw*(555) - *nLw* (488)) to *nLw*(555) and the last section in results was the conditions in which the radiance ratio of *nLw*(412) to *nLw*(555) was less than that of (*nLw*(555) - *nLw*(488)) to *nLw*(555).

The case of lower CDOM (included detritus) contribution to chlorophyll

The first approach tested that the condition in which the radiance ratio of *nLw*(412) to *nLw*(555) was greater than that of (*nLw*(555) - *nLw*(488)) to *nLw*(555) (blue circle samples in Fig. 5) was considered as lower CDOM (included detritus) contribution to chlorophyll. The re-plotted data in Fig. 6 were averaged over the area with different bin ranges of $a_{ph}(443)$ to determine the contribution of pigment to radiance (Fig. 6a-b). *nLw*(555) values ranged from ~0.5 to ~1 mw/cm²/μm/sr and *nLw*(443) from ~0.3 to ~0.7 mw/cm²/μm/sr, indicating large variations in the blue and green bands. With increasing chlorophyll concentration and
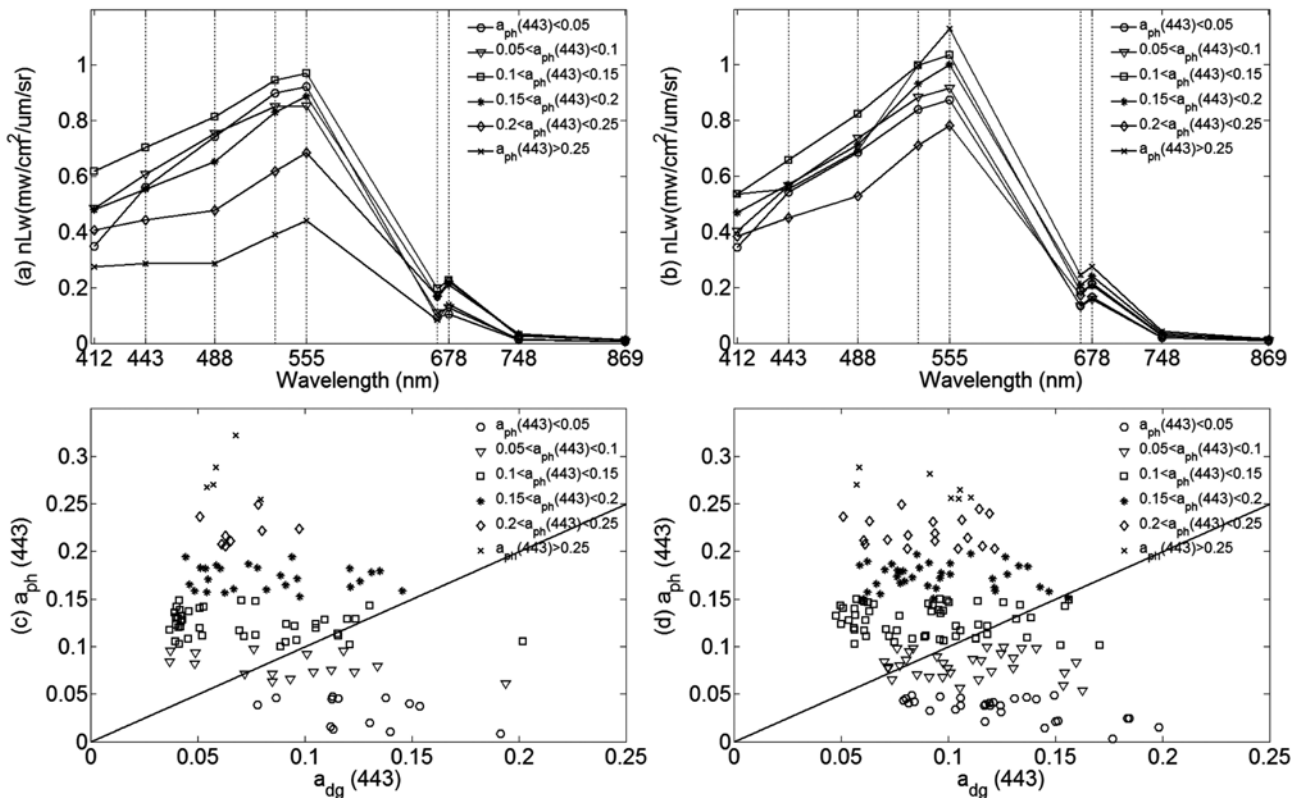
Fig. 6. The radiance spectral curve is plotted as a function of $a_{ph}(443)$ with different bin ranges (a and b) for red tide (left) and high satellite chlorophyll (right) waters. With an increase in $a_{ph}(443)$, the radiance values in the green and blue bands decreased (a and b) with increasing pigment absorption compared with those in CDOM (including detritus) absorption (c and d). Symbols indicate different phytoplankton absorption values

$a_{ph}(443)$ (Figs. 4a, b and 6a, b), $nLw(443)$ and $nLw(555)$ decreased and the slope between the blue and green bands showed a marked change. The slope between 412 and 488 nm was lower than that between 488 and 555 nm. These spectra were related to increased phytoplankton absorption rather than detritus/CDOM absorption (Fig. 6c, d). The spectra associated with lower a_{ph} values represented the linear slope between the blue and green bands due to the increasing influence of a_{dg}.

The correlation between the radiance ratio of $nLw(443)$ to $nLw(531)$ and the radiance ratio of $nLw(488)$ to $nLw(555)$ was tested with the data of Fig. 6 to distinguish true red tide water from false satellite high chlorophyll water (Fig. 7a). In Fig. 7b-d, the red tide samples (blue color) were consistent with relatively high $a_{ph}(443)$ values and FLH with varying chlorophyll concentrations. Decreased radiance blue band values in the red tide samples led to a lower slope in the blue bands and a higher slope in the green bands due to increased a_{ph} (Fig. 7e). The false satellite high chlorophyll samples (green color) correspond to relatively low $a_{ph}(443)$ and FLH

with varying chlorophyll concentrations (Fig. 7b-d). With an increased contribution of a_{dg} compared with a_{ph}, increased radiance values were observed in all blue and green bands (Fig. 7f), without a discernible slope between the blue and green bands.

The case of higher CDOM (included detritus) contributions to chlorophyll

Next, the second approach was tested that the condition in which the radiance ratio of $nLw(412)$ to $nLw(555)$ was less than that of ($nLw(555)$ - $nLw(488)$) to $nLw(555)$ (red square samples in Fig. 5) was considered as higher CDOM (included detritus) contribution to chlorophyll. Figure 8 was re-plotted with the data averaged over the area with different bin ranges of $a_{ph}(443)$. $nLw(555)$ ranged from ~0.7 to ~1.1 mw/cm^2/μm/sr and $nLw(443)$ ranged from ~0.2 to ~0.4 mw/cm^2/μm/sr. nLw values were slightly higher in the green band and lower in the blue band, compared with the results of Fig. 6. When $a_{ph}(443)$ and chlorophyll concentration (Figs. 4a, b and 8a, b) increased, $nLw(443)$ and $nLw(555)$
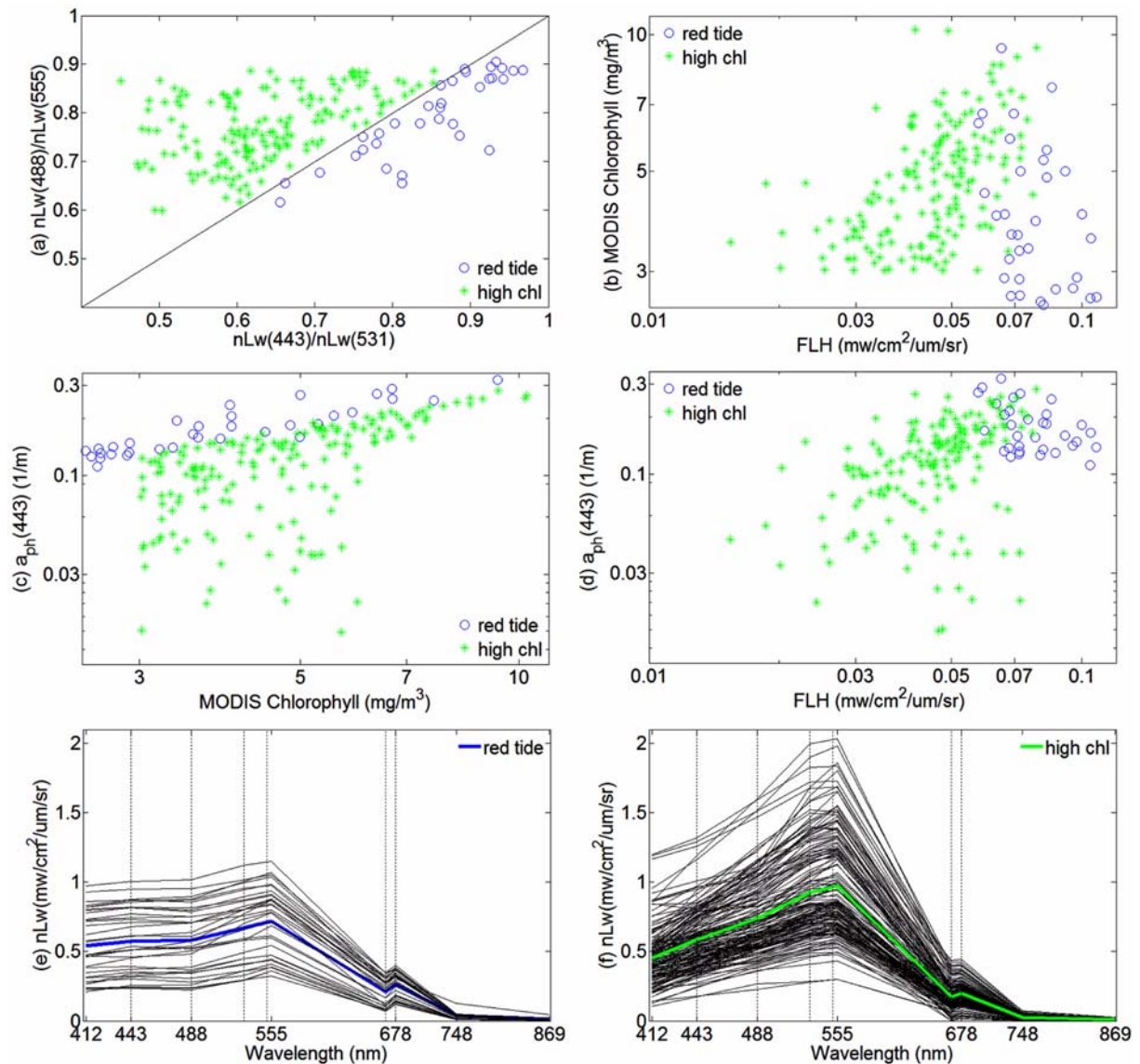
$\textcircled{2}$ Springer

Fig. 7. (a) The relationship between $nLw(488)/nLw(555)$ and $nLw(443)/nLw(531)$ was plotted to distinguish red tide water (blue color; $nLw(488)/nLw(555) > nLw(443)/nLw(531)$) from high satellite chlorophyll water (green color; $nLw(488)/nLw(555) \leq nLw(443)/nLw(531)$) using the data shown in Fig. 4. Red tide water had a strong influence on phytoplankton absorption and FLH with varying chlorophyll concentration (b-d). The red tide spectra (e) (the blue line shows the mean value) show that decreasing values at blue bands are related to increasing phytoplankton absorption in the blue band. The spectra for high chlorophyll water (f) (the green line shows the mean value) were correlated with relatively low phytoplankton absorption

decreased and the slope between the blue and green bands changed. The slope between 412 and 488 nm was lower than that between 488 and 555 nm; however, the results shown in Fig. 8c, d are less similar to those in Fig. 6c, d because the water was influenced mainly by increased a_{dg}.

The correlation between the ratio of $nLw(531)$ to $(nLw(488) + nLw(443))$ and the ratio of $nLw(488)$ to $(nLw(555) - nLw(488))$ was tested with the data of Fig. 8 to distinguish true red tide

water from false satellite high chlorophyll water (Fig. 9a). In Fig. 9b-d, the red tide samples (red color) were consistent with relatively high $a_{ph}(443)$, FLH, and chlorophyll concentration. Decreased $nLw(443)$ and $nLw(488)$ resulted in a different slope between the blue and green bands, with an increase in $a_{ph}(443)$ (Fig. 9e); however, the false satellite high chlorophyll samples (green color) were correlated with relatively low $a_{ph}(443)$, FLH, and chlorophyll concentration (Fig. 9b-d). The radiance spectra in Fig. 9f indicate that
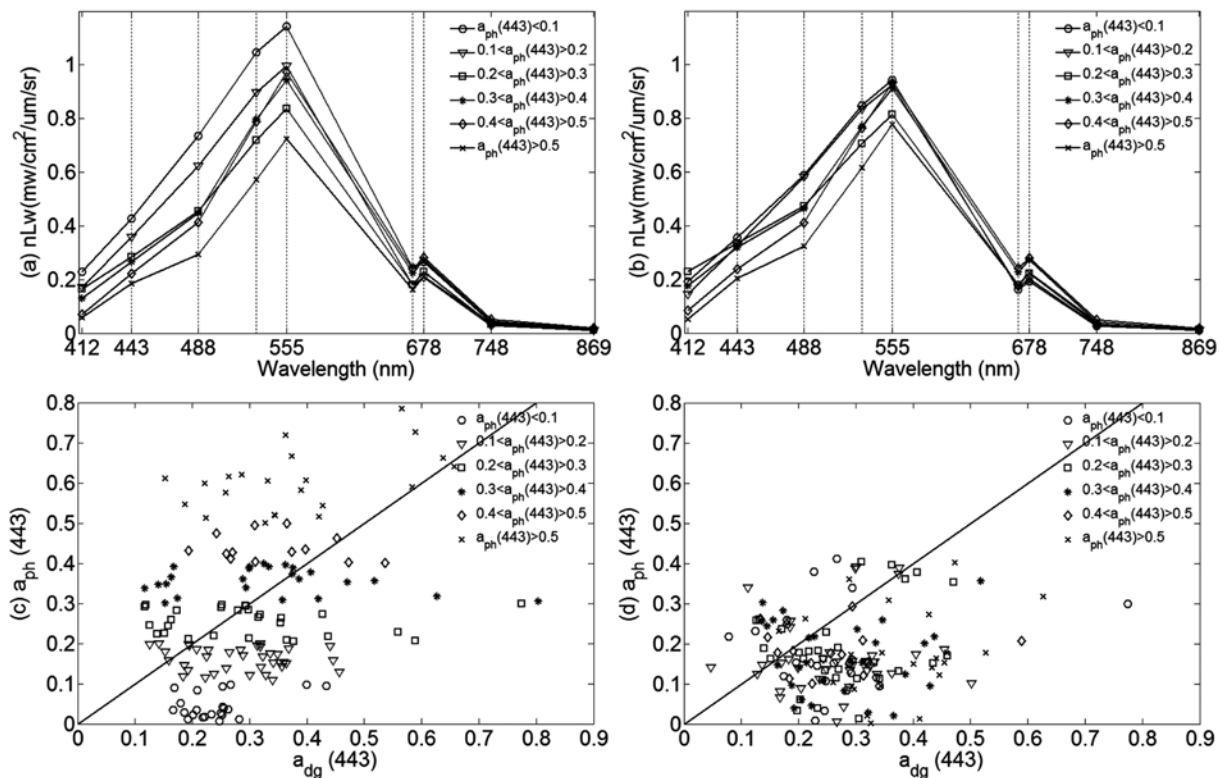
Fig. 8. The radiance spectral curve is plotted as a function of $a_{ph}(443)$ with different bin ranges (a and b) for red tide (left) and high satellite chlorophyll (right) waters. The relationship between $a_{ph}(443)$ and $a_{dg}(443)$ is plotted for various $a_{ph}(443)$ values (c, d). The radiance values in the green and blue bands are reduced for higher values of $a_{ph}(443)$, (a and b). Symbols indicate different phytoplankton absorption values

decreased $a_{ph}(443)$ produced a broad spectral curve without a hinge point at 488 nm.

4. Discussion

Red tide classification

In the present study, systematic spectral classification using multiple radiance-band ratios indicated a way to discriminate between red tide and non-red tide samples if distinct spectral correlations were obtained, as follows (Fig. 10):

Step 1: If the highest value of the radiance data is $nLw(555)$ with a fluorescence peak at 678 nm ($nLw(678)$ greater than $nLw(667)$), then the area is potentially a red tide; otherwise, the area consists of non-red tide water.

Step 2: If the ratio of $nLw(412)$ to $nLw(555)$ is greater than that of ($nLw(555) - nLw(488)$) to $nLw(555)$, then the area has a low contribution of detritus/CDOM to chlorophyll (continue to step 3); otherwise, the area has a high contribution of detritus/CDOM to chlorophyll (continue to step 4).

Step 3: If the ratio of $nLw(443)$ to $nLw(531)$ is greater than that of $nLw(488)$ to $nLw(555)$, then the area is a red

tide; otherwise, the area consists of non-red tide water.

Step 4: If the ratio of $nLw(531)$ to ($nLw(488) + nLw(443)$) is greater than that of $nLw(488)$ to ($nLw(555) - nLw(488)$), then the area is a red tide; otherwise, the area consists of non-red tide water.

The step 1 criterion (Figs. 3 and 4) detects waters with relatively high pigment concentrations that have the highest radiance values at the green and red bands. Increasing chlorophyll a concentrations are generally absorbed, with higher peaks at around 440-450 and 670-680 nm, and are reflected at 560-570 and 680-690 nm (Ahn et al. 2006; Dierssen et al. 2006; Sasaki et al. 2009). High satellite chlorophyll a concentrations and potential red tide water showed a radiance peak shifted to the green and red bands with higher $a_{ph}(443)$. Although the spectral shape and relative magnitude of the radiance, absorption, and backscattering varied depending on the organic/inorganic components, specific size, and pigment package effects, as well as several other factors (Letelier and Abbott 1996; Ahn and Moon 1998; Esaias et al. 1998; IOCCG 2000; Ahn et al. 2006; Dierssen et al. 2006), previous studies are in agreement that
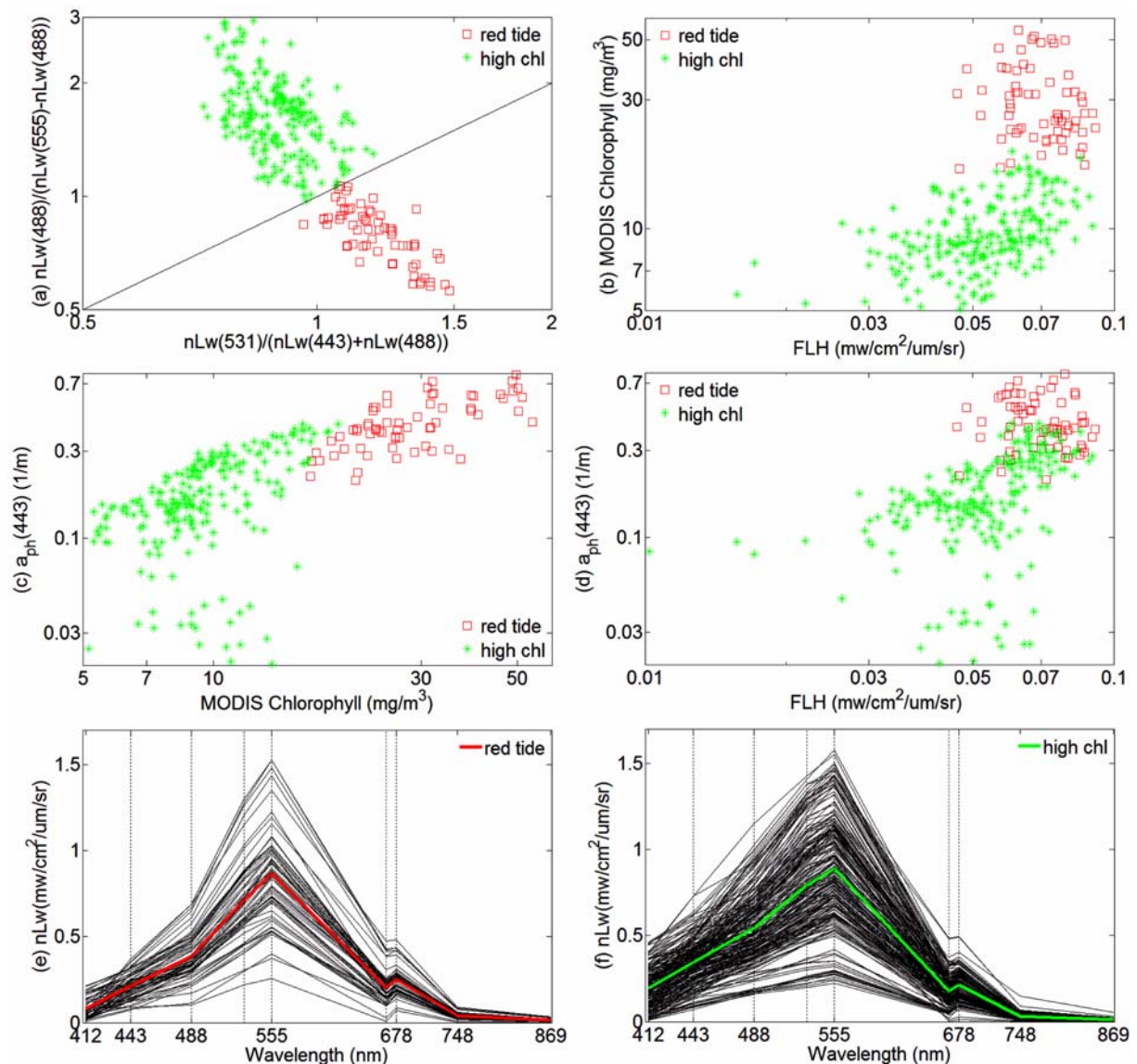
Fig. 9. (a) The relationship between $nLw(488)/(nLw(555) - nLw(488))$ and $nLw(531)/(nLw(443) + nLw(488))$ is plotted to distinguish red tide water (red color; $nLw(488)/(nLw(555) - nLw(488)) > nLw(531)/(nLw(443) + nLw(488))$) from high satellite chlorophyll water (green color; $nLw(488)/(nLw(555) - nLw(488)) \leq nLw(531)/(nLw(443) + nLw(488))$) based on the relatively high contribution of CDOM (detritus) to chlorophyll using the data shown in Fig. 4. Red tide water had a strong influence on phytoplankton absorption and FLH with varying chlorophyll (b-d). The red tide spectra (e) (the red line shows the mean value) showed that decreasing values in blue are related to increasing phytoplankton absorption in the blue band. The spectra for high chlorophyll water (f) (the green line shows the mean value) were correlated with relatively low phytoplankton absorption

the highest values of radiance at the green band are observed with increasing organic/inorganic particle concentrations, and the highest values at the blue band are observed with decreasing organic/inorganic particle concentrations. Morel and Maritorena (2001) and Werdell and Bailey (2005) showed that the peak radiance shifts from shorter wavelengths (violet to blue bands) to longer wavelengths (green band) with increasing chlorophyll a concentrations in surface

water. Sasaki et al. (2009) showed a similar shift in a study in Ariake Bay, although the authors explained the shift in terms of turbidity and CDOM.

The step 2 criterion (Figs. 4 and 5) is designed to discriminate between optically contrasting waters, related to relatively high or low contributions of detritus/CDOM to chlorophyll. *C. polykrikoides* blooms in Korean coastal waters are found in inshore waters as well as clear, offshore waters (Kang et
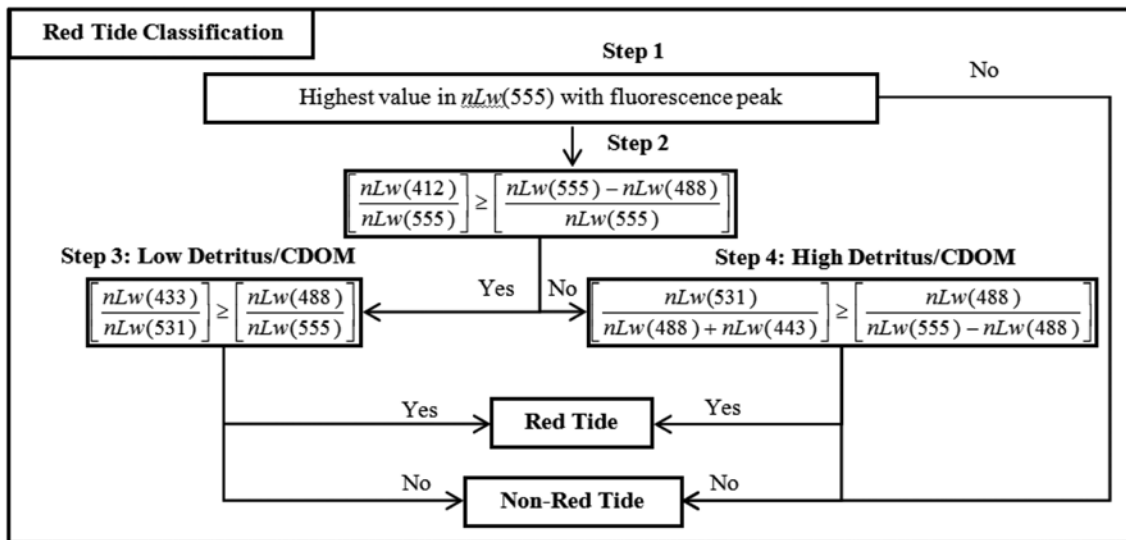
Fig. 10. Process employed to classify red tides using a four-step spectral classification

al. 2002; Suh et al. 2004; Ahn et al. 2006; Lee 2006; Shanmugam et al. 2008). Clear water is less sensitive to the influence of suspended particulate material and CDOM, whereas inshore water is strongly influenced by CDOM and organic/inorganic material (Fig. 4). The spectral curve obtained for optically complex water conditions was influenced by increased absorption in blue bands, whereas clear offshore waters showed less absorption by pigments or CDOM but increased absorption in blue bands as a result of water scattering (Carder et al. 1999; IOCCG 2000; Sathyendranath et al. 2001; Siegel et al. 2005). The difference in slope between LSCW and HSCW in Fig. 4i, j was attributed to different absorption effects, particularly in terms of a_{dg}. The step 2 criterion was applied to separate the two spectra. Separation using the two band ratios was based on the premise that an area with a radiance ratio of $nLw(412)$ to $nLw(555)$ greater than that of ($nLw(555)$ - $nLw(488)$) to $nLw(555)$ had a lower contribution of detritus/CDOM to chlorophyll (blue color in Fig. 5). An area with a radiance ratio of $nLw(412)$ to $nLw(555)$ less than that of ($nLw(555)$ - $nLw(488)$) to $nLw(555)$ was considered to have a higher contribution of detritus/CDOM to chlorophyll (red color in Fig. 5). The results obtained after applying step 2 were well matched as shown in the results of Fig. 4.

The step 3 criterion (Figs. 6 and 7) was employed to discriminate red tide water from non-red tide water in the case of a relatively low contribution of CDOM (included detritus) to chlorophyll. The binned radiance spectra in Fig. 6a, b indicate that the spectra with increased $a_{ph}(443)$ and

FLH produced a lower slope between 412 and 488 nm than between 488 and 555 nm, and was connected by a hinge point at 488 nm. This result was caused by an increase in pigment concentration. When $a_{ph}(443)$ and FLH decreased, the radiance signal diminished steeply from the green to blue bands, without the hinge point at 488 nm; these results were influenced by an increase in a_{dg} (Fig. 6). After applying step 3, the radiance spectra of the red tide in Fig. 7e showed reduced radiance values in the blue and green bands, and increased values in the red band, compared with the non-red tide radiance spectra (Fig. 7f). These results reflect the presence of enhanced pigment concentrations (Fig. 7b-d; Stramski and Kiefer 1991; Dierssen et al. 2006; Sasaki et al. 2008).

The step 4 criterion (Figs. 8 and 9) was employed to determine red tide water from non-red tide water in the case of a relatively high contribution of CDOM (detritus) to chlorophyll. With increasing $a_{ph}(443)$ and FLH, the averaged radiance spectra in Fig. 8a, b showed similar results to those in Fig. 6a, b, i.e., a lower slope between 412 and 488 nm than between 488 and 555 nm, connected by a hinge point at 488 nm. After applying step 4 (Fig. 9), the red tide water was observed based on enhanced chlorophyll, FLH, and phytoplankton absorption. Decreased radiance values at 443 and 488 nm, with a hinge point at 488 nm (Fig. 9e), indicated an increase in a_{ph} compared with that in non-red tide water.

After applying the red tide classification from steps 1-4 (Fig. 10), the spectral curves of red tide and non-red tide
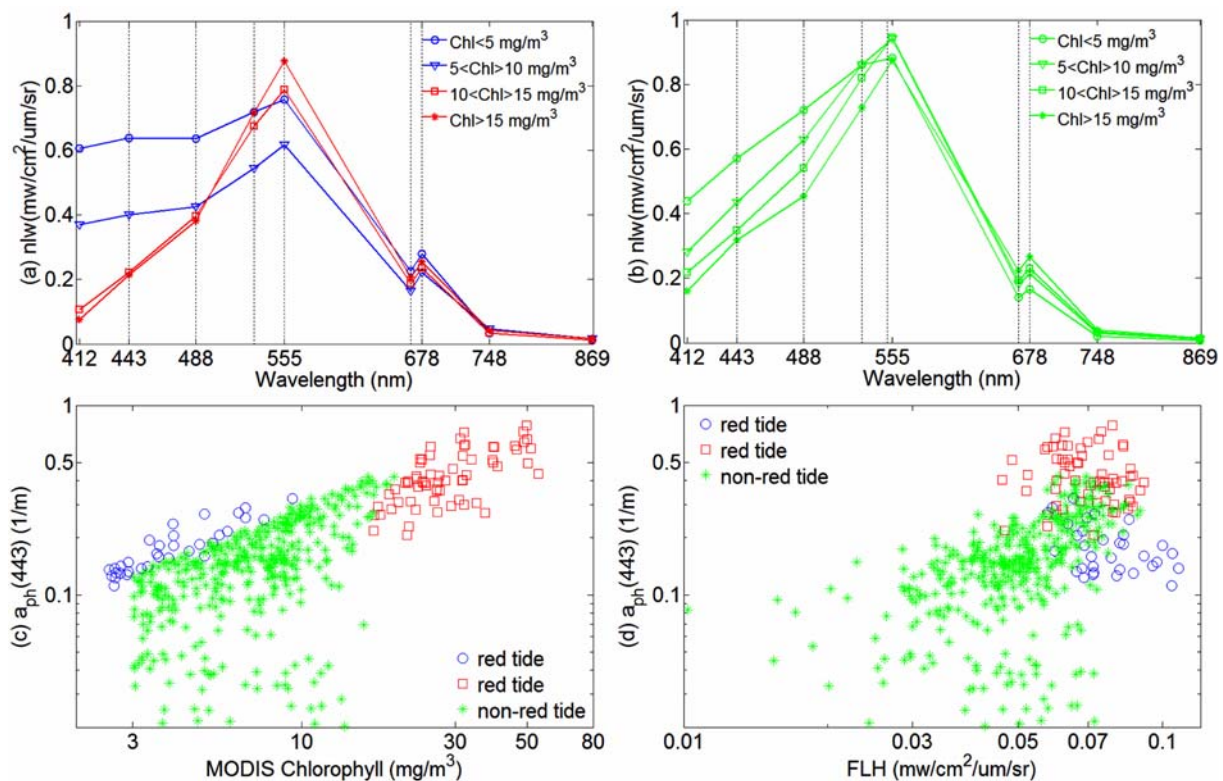
Fig. 11. Spectral variability averaged over the study area with different chlorophyll *a* concentration bin ranges, showing (a) the spectra of red tides that satisfy steps 1 to 4 (blue color indicates a low contribution of CDOM to chlorophyll; red color indicates a high contribution) and (b) non-red tide water after applying steps 1 to 4. The red tide water was correlated with enhanced chlorophyll, FLH, and phytoplankton absorption (c and d)

water were plotted using the different average bin ranges of chlorophyll concentration (Fig. 11). The spectral response of red tide and non-red tide waters revealed two dominant peaks in the green and red bands (Fig. 11a, b). A bell-shaped spectral curve was observed between the green and red wavelengths due to increasing particle concentrations (including chlorophyll; O'Reilly et al. 2000; Werdell and Bailey 2005). The higher radiance values in the blue bands were influenced by the relative low contribution of CDOM to chlorophyll. The lower radiance values in the blue bands were influenced by the relatively high contribution of CDOM to chlorophyll.

C. polykrikoides blooms in SSK show higher and lower radiance values at 555 and 440 nm, respectively, than do diatom blooms, due to increased pigment backscattering in the green band and chlorophyll absorption in the blue band (Ahn and Moon 1998; Ahn et al. 2006). Optically, larger phytoplankton species have lower absorption per mass of chlorophyll *a* than do smaller phytoplankton, because of packaging effects within the cells (Bricaud et al. 1995; Ciotti et

al. 2002). Relatively high absorption and backscattering in dense *C. polykrikoides* blooms may explain the difference between green and blue bands, whereas high-chlorophyll water influenced by CDOM and organic/inorganic matter may produce optically broader reflectance spectra (Fig. 11a, b; Dierssen et al. 2006). Red tide spectra classified from steps 1-4 (Fig. 10) showed enhanced phytoplankton absorption and FLH with varying chlorophyll concentrations (Fig. 11c, d).

Case studies: Spatial and temporal variations of HAB in the South Sea of Korea

The true color composite obtained on August 19, 2002 (Fig. 12) showed several areas of discolored water, and dark and bright colors varied with MODIS chlorophyll *a* concentration, FLH, and a_{ph}(443). In the present study area, the visual appearance of *C. polykrikoides* blooms is discolored water ranging in color from blue to dark red/brown (Ahn and Shanmugam 2006), with relatively high chlorophyll concentrations. Increased absorption of chlorophyll and non-living particles generally induce a reduction in radiance at
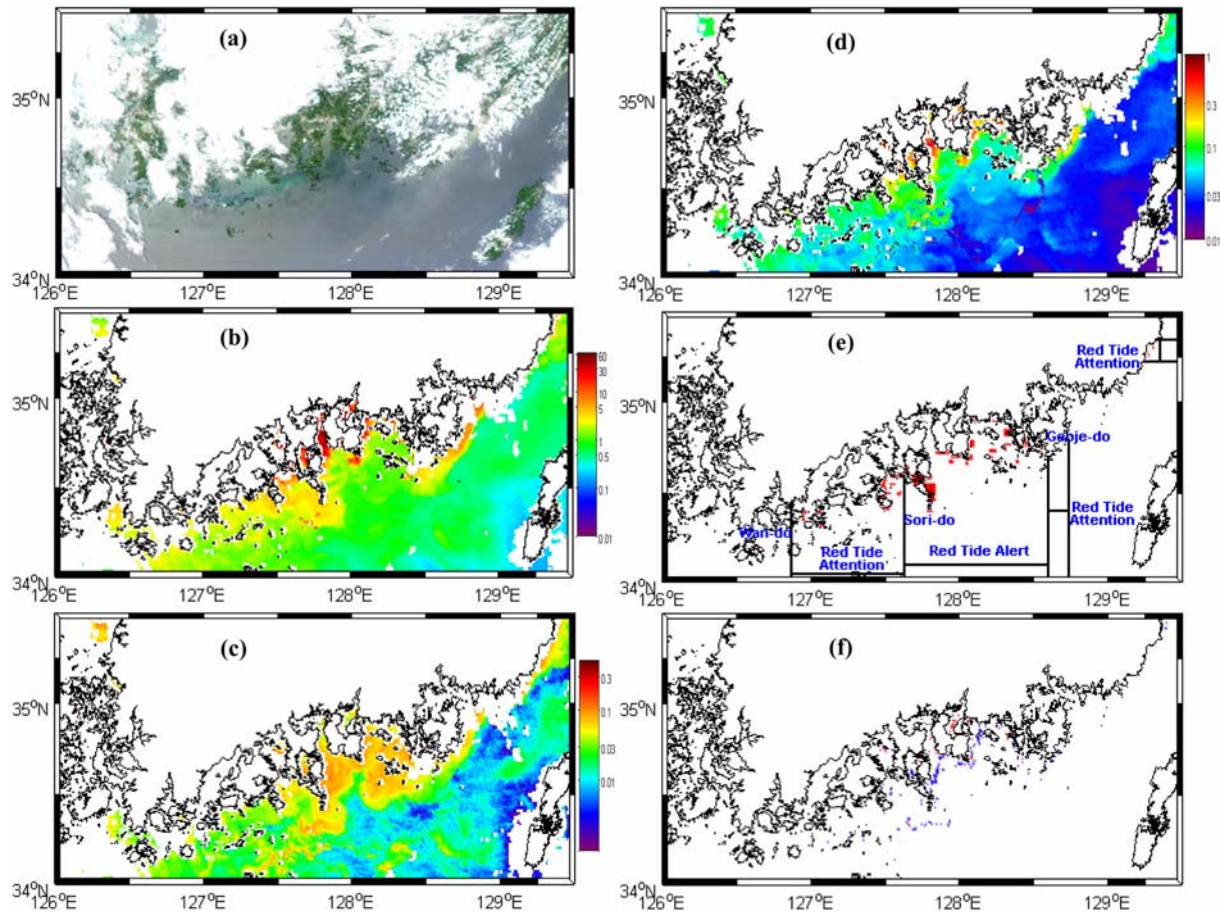
Fig. 12. Maps of (a) true color composite, (b) MODIS chlorophyll *a* concentration (mg/m^3), (c) FLH (mw/cm^2/μm/sr), and (d) a_{ph}(443) (1/m) for August 19, 2002. (e) Red areas represent spatial information for the occurrence of harmful algal blooms (HAB) (NFRDI 2004). (f) After applying the spectral classification (Fig. 10), the spatial extent of algal blooms was reduced and well correlated with the documented red tide map (e) (a relatively low contribution of CDOM to chlorophyll (blue color) and a relatively high contribution of CDOM to chlorophyll (red color))

blue wavelengths, with no scattering of light that visually appears in water discolored to dark hues or black (Dierssen et al. 2006). The water containing enhanced chlorophyll, FLH, and a_{ph}(443) was well matched with areas of discolored water (Fig. 12a-d).

As shown in Fig. 12e, *C. polykrikoides* blooms were observed between Sori-do and Geojo-do, as red tide "alert" areas, and between Wan-do and Sori-do, east of Geojo-do, and northeast of Busan as red tide "attention" areas; the cell density of *C. polykrikoides* was 10-15,000 cell/ml (NFRDI 2004). Lee (2006) noted that increased rainfall during early August 2002 (salinity: 26.5 psu at Geomo-do on August 19, 2002) caused increasing nutrient concentration. The red tide "attention" area between Wan-do and Sori-do appeared bright blue and blue-green with a chlorophyll *a* concentration of 2-10 mg/m^3, 0.02-0.09 mw/cm^2/μm/sr FLH, and 0.05-

0.2 1/m a_{ph}(443). Around Geoje-do, water with a bright brown color bordered an offshore area with moderate chlorophyll concentrations (~0.5 mg/m^3) (Fig. 12a, b). In the red tide "alert" area (Fig. 12e), two distinct color features (bright brown-green and blue-green) between Yeosu and Namhae-do bordered an area with relatively high concentrations of chlorophyll *a* (>10 mg/m^3). A brown-red color was observed between Namhae-do and Sang-do (Fig. 12a, b). The region near Namhae-do was influenced by relatively high chlorophyll, FLH, and a_{ph}(443). The red tide area near Tongyeong and Geoje-do was spatially correlated with moderate chlorophyll *a* concentrations (1-3 mg/m^3) but only slightly increased FHL (~0.1 mw/cm^2/μm/sr; Fig. 12b, c).

Figure 12f shows the *C. polykrikoides* bloom areas after applying steps 1-4 (Fig. 10). Blue areas indicate a lower

contribution of CDOM to chlorophyll, whereas red areas indicate a higher contribution of CDOM to chlorophyll (Fig. 10). The area with the highest potential for *C. polykrikoides* bloom (Fig. 12f) coincided with the area of red tide occurrence (Fig. 12e) and a low contribution of detritus/CDOM to chlorophyll. The inshore area between Yeosu and Geoje-do was correlated with a relatively high contribution of CDOM to chlorophyll (Fig. 12f). The water between Naro-do and Sori-do showed an increased chlorophyll concentration and extended out across the shelf, beyond the estimated red tide area (Fig. 12b, f). This finding may be related to decreasing pigment concentrations and was only found in small patches (Fig. 12b-d, f). Table 3 provides the six different red tide detection algorithms and our analysis (spectral classification) between reference and satellite data (Tables 1 and 2). On August 19, 2002, user accuracy for the *C. polykrikoides* bloom and non-red tide using spectral classification was estimated to be 47.93% and 99.24%. A 48% of the *C. polykrikoides* bloom was flagged (true positive, 104 pixels) but 52% of that masked out (false negative, 113 pixels). In total, 142 pixels (false positive) were over-estimated as *C. polykrikoides* blooms (precision of 42.28%).

The entire apparent true-color image obtained on September 8, 2002 (Fig. 13), after Typhoon Rusa had passed over the SSK on August 31, 2002 (Lee and Niller 2003), contained discolored waters that differed between the western and eastern parts of the study area, varying with chlorophyll *a* concentrations, FLH, and a_{ph}(443). Surprisingly, the water with high chlorophyll, FLH, and a_{ph} extended offshore from the study area (Fig. 13b-d), matching the true color image (Fig. 13a). Lee and Niller (2003) reported that Typhoon Rusa produced well-mixed offshore water that intruded nearshore areas along the southern coast of Korea, driven
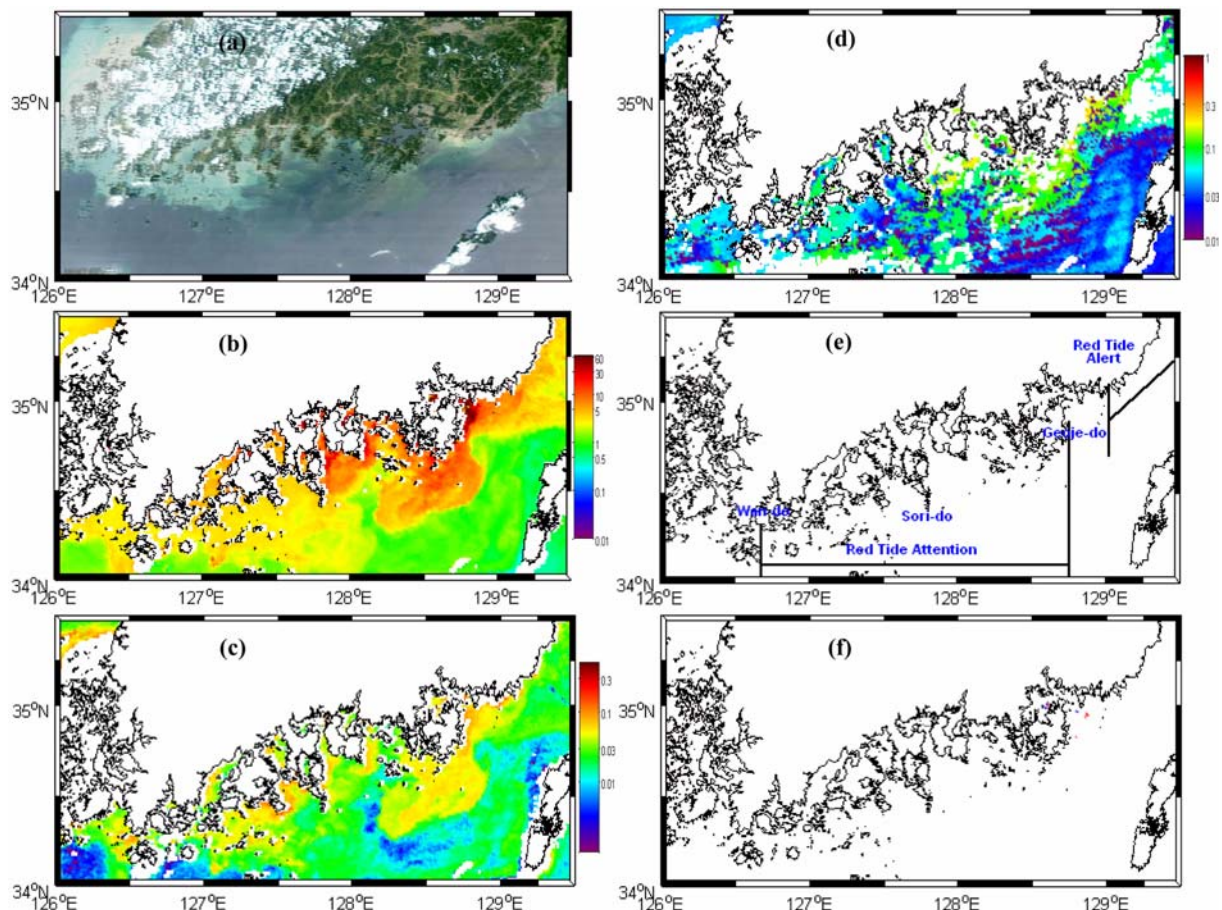

Fig. 13. Maps of (a) true color composite, (b) MODIS chlorophyll *a* concentration (mg/m³), (c) FLH (mw/cm²/μm/sr), and (d) a_{ph}(443) (1/m) for September 8, 2002. (e) Red areas represent spatial information for the occurrence of harmful algal blooms (HAB) (NFRDI 2004). (f) After applying the spectral classification (Fig. 10), the spatial extent of algal blooms was reduced and well correlated with the documented red tide map (e) (a relatively low contribution of CDOM to chlorophyll (blue color) and a relatively high contribution of CDOM to chlorophyll (red color))

by a strong northeasterly wind. The bright yellow or brown color in the red tide "attention" area between Wan-do and Sori-do (Fig. 13a, e) represented storm-resuspended sediment, which produced high particulate backscattering (relatively low chlorophyll concentration, FLH, and $a_{ph}(443)$). Although chlorophyll *a* concentrations showed a marked increase over the entire study area, particularly offshore from Geojo-do (Fig. 13b), *C. polykrikoides* blooms were observed between Wan-do and Geoje-do as a red tide "attention" area

and northeast of Busan as a red tide "alert" area (Fig. 12e), with a relatively low cell density (50-1,500 cell/ml; NFRDI 2004).

After the passing of Typhoon Rusa, relatively low pigment concentrations (FLH <0.1 mw/cm^2/μm/sr and $a_{ph}(443)$ <0.2 1/m; Fig. 13c, d) were found around Sori-do to Geoje-do and the red tide "alert" areas, along with enhanced chlorophyll *a* concentrations (>5 mg/m^3; Fig. 13b), related to the large amount of rainfall and input of fresh water from

Table 3. Accuracy of each red tide detection method

Method	Events	TP	FN	FP	TN	Total events	Total Accuracy (%)	Precision (%)	User Accuracy for *C. polykrikoides* (%)	User Accuracy for non-red tide (%)
Chloro-phyll Anomaly	Aug. 19, 2002	54	146	1029	16839	18068	93.50	4.99	27.00	94.24
	Sep. 08, 2002	0*	0*	1188	17463	18651	93.63	-999	-999	93.63
	Aug. 22, 2003	46	164	1376	15913	17499	91.20	3.23	21.90	92.04
	Aug. 28, 2004	33	31	1815	9643	11522	83.98	1.79	51.56	84.16
	Aug. 21, 2007	27	133	979	20567	21706	94.88	2.68	16.88	95.46
$b_{bp}/b_{bp\_}$ morel	Aug. 19, 2002	118	99	5428	13297	18942	70.82	2.13	54.38	71.01
	Sep. 08, 2002	0*	0*	12902	6544	19446	33.65	-999	-999	33.65
	Aug. 22, 2003	144	87	5513	12801	18545	69.80	2.55	62.34	69.90
	Aug. 28, 2004	37	27	3605	8297	11966	69.65	1.02	57.81	69.71
	Aug. 21, 2007	95	69	7821	15404	23389	66.27	1.20	57.93	66.33
FLH	Aug. 19, 2002	14	184	49	17792	18039	98.71	22.22	7.07	99.73
	Sep. 08, 2002	0*	0*	106	18080	18186	99.42	-999	-999	99.42
	Aug. 22, 2003	10	201	48	15781	16040	98.45	17.24	4.74	99.70
	Aug. 28, 2004	12	47	37	10858	10954	99.23	24.49	20.34	99.66
	Aug. 21, 2007	10	140	175	21311	21636	98.54	5.41	6.67	99.19
SS	Aug. 19, 2002	128	89	3894	14831	18942	78.97	3.18	58.99	79.20
	Sep. 08, 2002	0*	0*	6091	13355	19446	68.68	-999	-999	68.68
	Aug. 22, 2003	107	124	3934	14380	18545	78.12	2.65	46.32	78.52
	Aug. 28, 2004	46	18	3370	8532	11966	71.69	1.35	71.88	71.69
	Aug. 21, 2007	67	97	5486	17739	23389	76.13	1.21	40.85	76.38
TSF	Aug. 19, 2002	46	171	846	17879	18942	94.63	5.16	21.20	95.48
	Sep. 08, 2002	0*	0*	4854	14592	19446	75.04	-999	-999	75.04
	Aug. 22, 2003	20	211	261	18053	18545	97.45	7.12	8.66	98.57
	Aug. 28, 2004	32	32	856	11046	11966	92.58	3.60	50.00	92.81
	Aug. 21, 2007	25	139	179	23046	23389	98.64	12.25	15.24	99.23
FRTD	Aug. 19, 2002	40	177	566	18159	18942	96.08	6.60	18.43	96.13
	Sep. 08, 2002	0*	0*	1336	18110	19446	93.13	-999	-999	93.13
	Aug. 22, 2003	62	102	1670	17932	19766	91.04	3.58	37.80	91.48
	Aug. 28, 2004	24	40	1059	10843	11966	90.82	2.22	37.50	91.10
	Aug. 21, 2007	13	151	719	22506	23389	96.28	1.78	7.93	96.90
Spectral classifica-tion	Aug. 19, 2002	104	113	142	18583	18942	98.65	42.28	47.93	99.24
	Sep. 08, 2002	0*	0*	8	19438	19446	99.96	-999	-999	99.96
	Aug. 22, 2003	106	125	134	18180	18545	98.60	44.17	45.89	99.27
	Aug. 28, 2004	30	34	256	11646	11966	97.58	10.49	46.88	97.85
	Aug. 21, 2007	79	85	280	22945	23389	98.44	22.01	48.17	98.79

*No reference map of *C. polykrikoides* was available for Sept. 8, 2002 (NFRDI, 2004).
-999 : No calculation due to the lack of a *C. polykrikoides* reference map (NFRDI, 2004).

rivers (Lee and Niller 2003; Lee 2006). This area was no longer seen after applying spectral classification (Fig. 13f). Offshore water mixed by a typhoon or northeasterly storm may diminish the extent of *C. polykrikoides* blooms as a result of reduced stratification of the water column (Ryan et al. 2005; Lee 2008). Increased vertical mixing can optically increase CDOM and detritus absorption at shorter wavelengths, producing false satellite high chlorophyll water as "noise". On September 8, 2002, precision and user accuracy of *C. polykrikoides* bloom was not estimated because of the lack of a reference map for the *C. polykrikoides* bloom area. Only 8 pixels (false positive) were over-estimated as *C. polykrikoides* blooms (Table 3).

On August 22, 2003 (Fig. 14), various discolored water (brown, blue, and dark hues) covered the area with enhanced chlorophyll, FLH, and $a_{ph}(443)$. The areas south of Busan and near Dolsan-do, as well as the west coast, appeared

as bright brown or yellow, with enhanced chlorophyll concentrations (>7 mg/m^3), FLH (>0.08 mw/cm^2/μm/sr), and $a_{ph}(443)$ (>0.1 1/m). Relatively high chlorophyll containing water in the southwest of the study area visually appeared as blue and dark green colors, and extended to offshore areas. *C. polykrikoides* blooms were observed between Wan-do and Geogeum-do, and west of Sori-do and Geoje-do as red tide "alert" areas, and between Geogeum-do and west of Sori-do as red tide "attention" areas; the density of *C. polykrikoides* was 25-8,200 cell/ml (Fig. 14e; NFRDI 2004). The red tide "alert" area between Wan-do and Geogeum-do (Fig. 14e), which was blue and brown in color, showed high chlorophyll concentrations (3-20 mg/m^3) and moderate FLH and $a_{ph}(443)$ (0.03-0.08 mw/cm^2/μm/sr and 0.09-0.2 1/m, respectively). The area between Dolsan-do and Namhae-do was bordered by a bright brown-green color, with higher chlorophyll *a* concentrations, FLH, and $a_{ph}(443)$
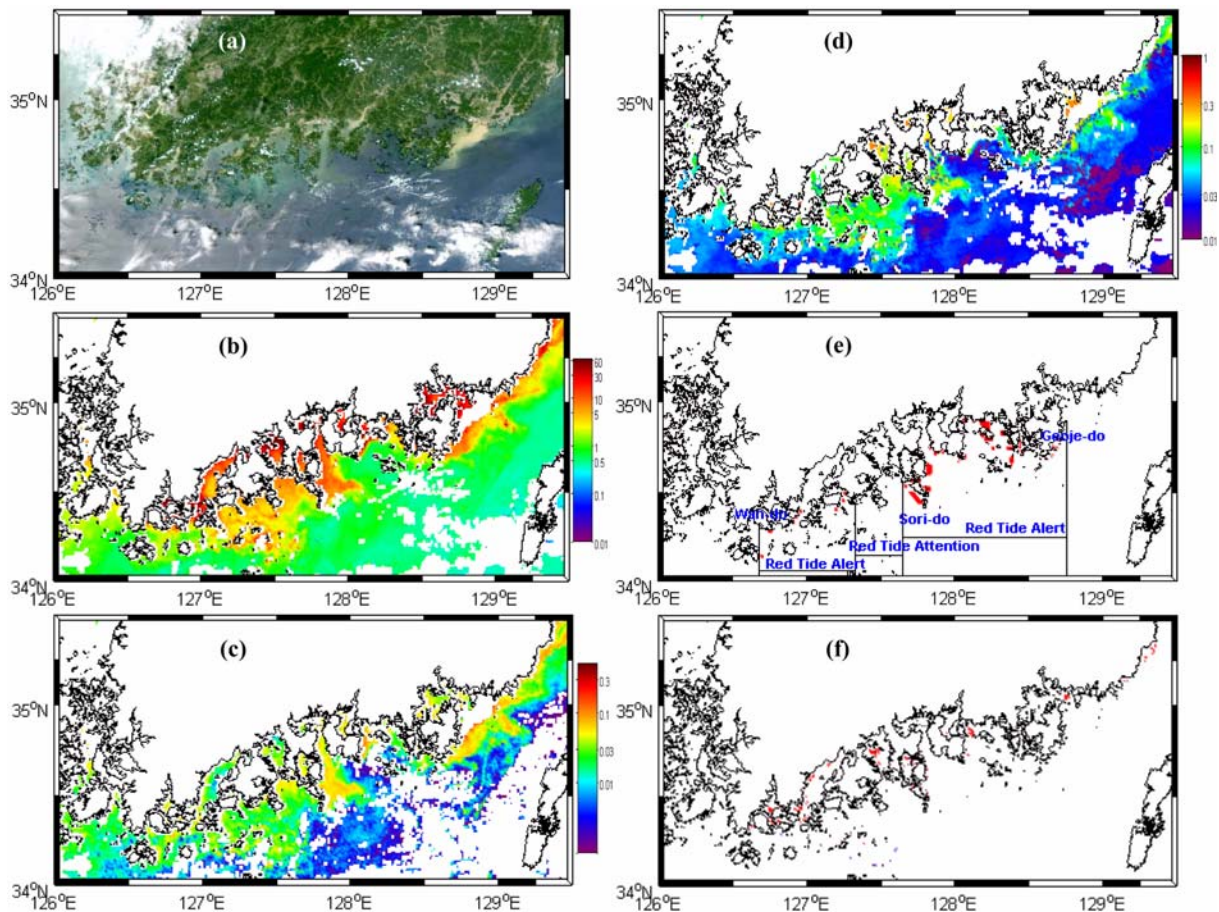

Fig. 14. Maps of (a) true color composite, (b) MODIS chlorophyll *a* (mg/m^3), (c) FLH (mw/cm^2/μm/sr), and (d) $a_{ph}(443)$ (1/m) for August 22, 2003. (e) Red areas represent spatial information for the occurrence of harmful algal blooms (HAB) (NFRDI 2004). (f) After applying the spectral classification (Fig. 10), the spatial extent of algal blooms was reduced and well correlated with the documented red tide map (e) (a relatively low contribution of CDOM to chlorophyll (blue color) and a relatively high contribution of CDOM to chlorophyll (red color))

(>7 mg/m^3, >0.09 mw/cm^2/μm/sr, and >0.2 1/m, respectively). The area around Sang-do visually appeared as a dark green-blue color and showed relatively high chlorophyll *a* concentrations and FLH (>3 mg/m^3 and 0.9 mw/cm^2/μm/sr, respectively; Fig. 14b, c). High concentrations of chlorophyll *a* (5-10 mg/m^3; Fig. 14a, b) were observed around Geoje-do, visually appearing as bright brown. The red tide "attention" area between Geogeum-do and Sori-do (Fig. 14e) appeared as bright blue and green colors, with chlorophyll *a* concentrations of 3-7 mg/m^3, FLH of 0.02-0.05 mw/cm^2/μm/sr, and a_{ph}(443) of 0.01-0.2 1/m (Fig. 14a-d).

After applying steps 1-4 (Fig. 14f), the red tide area further contracted to around Wan-do and between Sori-do and Geoje-do (red tide "alert" area; NFRDI 2004), showing an increase in pigment concentrations. Although offshore waters showed an increase in pigment concentration, the potential bloom area disappeared, with only small patches

remaining. On August 22, 2003 (Table 3), user accuracy for the *C. polykrikoides* bloom and non-red tide using spectral classification was estimated to be 45.89% and 99.27%. A 46% of the *C. polykrikoides* bloom was flagged (true positive, 106 pixels) but 54% of that masked out (false negative, 125 pixels). In total, 134 pixels (false positive) were over-estimated as *C. polykrikoides* bloom (precision of 44.17%).

On August 28, 2004 (Fig. 15), most of the offshore area was masked by cloud (Fig. 15a). *C. polykrikoides* blooms were observed between Yeosu and Namhae-do as a red tide "alert" area and between Wan-do and Yeosu and Yokji-do, and at Geoje-do as a red tide "attention" area (Fig. 15e), with relatively low cell density (25-700 cell/ml; NFRDI 2005). NFRDI (2005) noted that limited observations were carried out because of severe weather conditions in the study area. However, high chlorophyll concentrations (>3
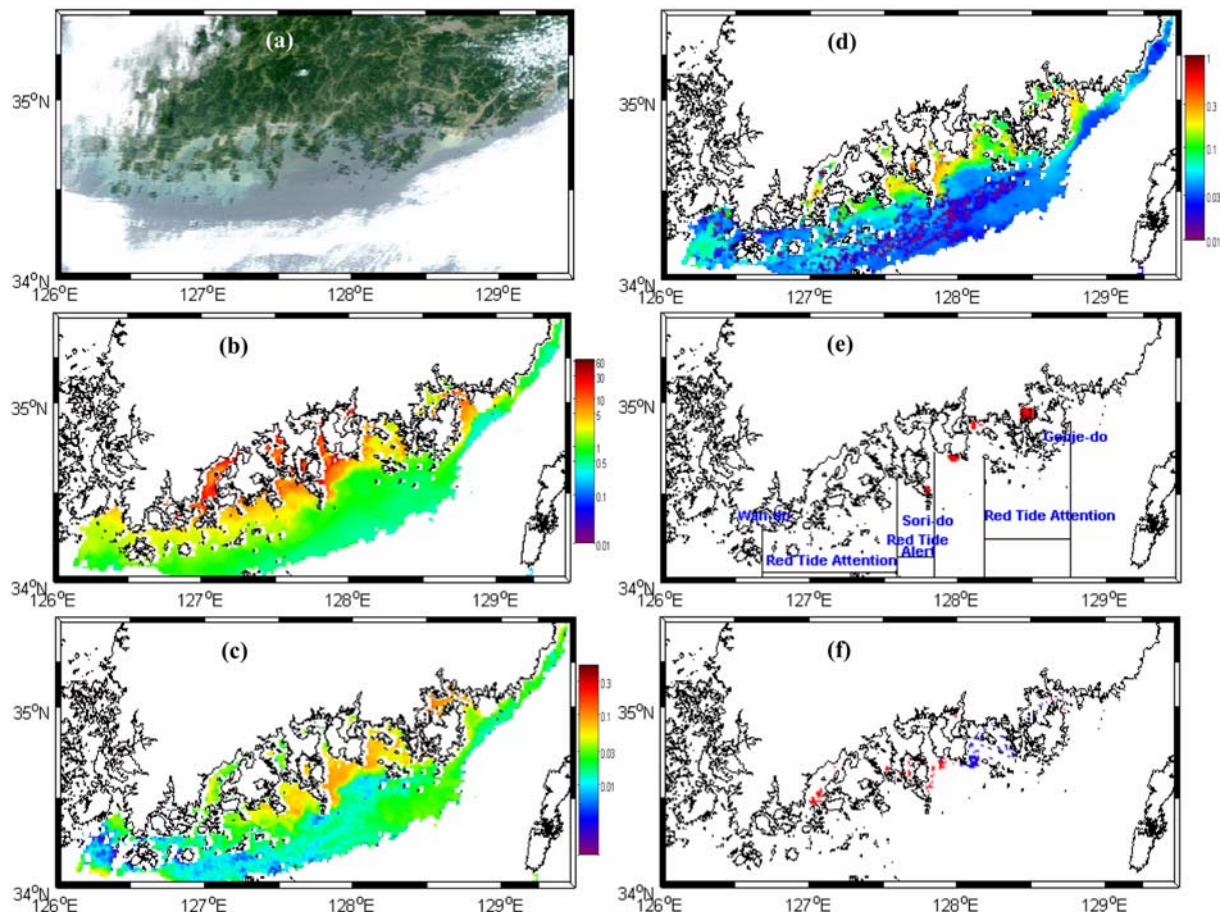

Fig. 15. Maps of (a) true color composite, (b) MODIS chlorophyll *a* concentration (mg/m^3), (c) FLH (mw/cm^2/μm/sr), and (d) a_{ph}(443) (1/m) for September 28, 2004. (e) Red areas represent spatial information for the occurrence of harmful algal blooms (HAB) (NFRDI 2005). (f) After applying the spectral classification (Fig. 10), the spatial extent of algal blooms was reduced and well correlated with the documented red tide map (e) (a relatively low contribution of CDOM to chlorophyll (blue color) and a relatively high contribution of CDOM to chlorophyll (red color))

mg/m³) and a_{ph}(443) (>0.1 mw/cm²/μm/sr; Fig. 15b, d), apparent as bright blue and brown colors (Fig. 15a), were observed between Wan-do and Sori-do as a red tide "attention" area (Fig. 15e). It was difficult to discern the color between Sang-do and Geoje-do (chlorophyll *a* concentration: 3-7 mg/m³) because of hazy conditions (Fig. 15a). Enhanced chlorophyll *a* concentrations (>7 mg/m³), FLH (>0.1 mw/cm²/μm/sr), and a_{ph}(443) (>0.2 1/m), showing bright blue and brown colors (Fig. 15b-d), were observed between Sori-do and Namhae-do as a red tide "alert" area (Fig. 15e). After applying spectral classification (Fig. 10), the red tide area was restricted to Sori-do (red tide "alert" area), Namhae-do, and Tongyeong, with relatively enhanced FLH and a_{ph}(443) (Fig. 15c, d). On August 28, 2004 (Table 3), user accuracy for the *C. polykrikoides* bloom and non-red tide using spectral classification was estimated to be

46.88% and 97.85%. A 47% of the *C. polykrikoides* bloom was flagged (true positive, 30 pixels) but 53% of that masked out (false negative, 34 pixels). A total of 256 pixels (false positive) were over-estimated as a *C. polykrikoides* bloom (precision of 10.49%).

On August 21, 2007 (Fig. 16), increased concentrations of chlorophyll were found for most of the discolored water in inshore areas. *C. polykrikoides* blooms between Wan-do and Yeosu were classed as a red tide "attention" area, and those between Yeosu and Geoje-do as a red tide "alert" area (Fig. 16e), with a high cell density (10-12,240 cell/ml; http://www.nfrdi.re.kr/redtideInfo). The red tide "attention" area (Fig. 16e) was bright/dark blue-green in color with moderate chlorophyll *a* concentrations (2-5 mg/m³), FLH (0.01-0.04 mw/cm²/μm/sr), and a_{ph}(443) (0.05-0.2 1/m; Fig. 16b-d). The red tide "alert" area between Sori-do and Geoje-do
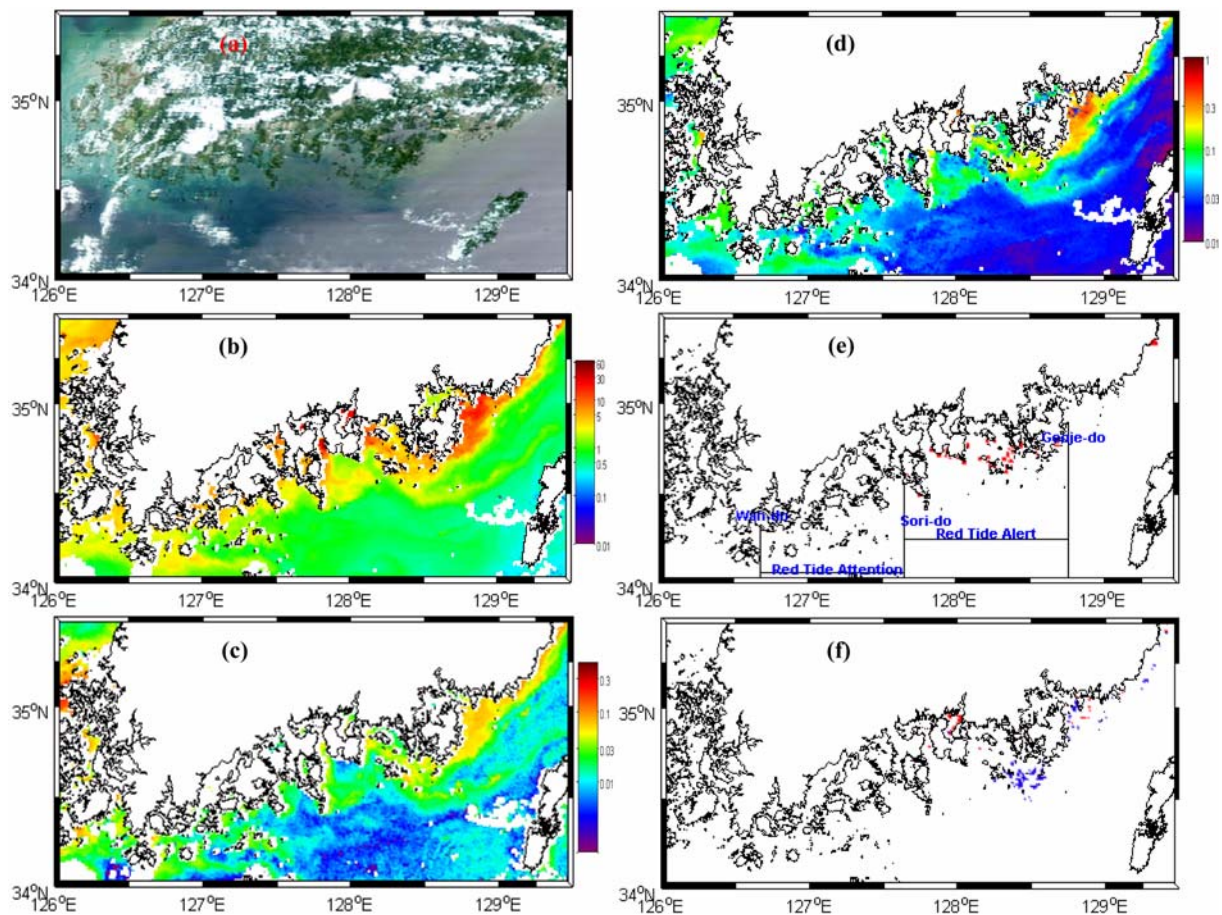

Fig. 16. Maps of (a) true color composite, (b) MODIS chlorophyll *a* concentration (mg/m³), (c) FLH (mw/cm²/μm/sr), and (d) a_{ph}(443) (1/m) for August 21, 2007. (e) Red areas represent spatial information for the occurrence of harmful algal blooms (HAB) (Lim et al. 2008; http://www.nfrdi.re.kr/redtideInfo). (f) After applying the spectral classification (Fig. 10), the spatial extent of algal blooms was reduced and well correlated with the documented red tide map (e) (a relatively low contribution of CDOM to chlorophyll (blue color) and a relatively high contribution of CDOM to chlorophyll (red color))
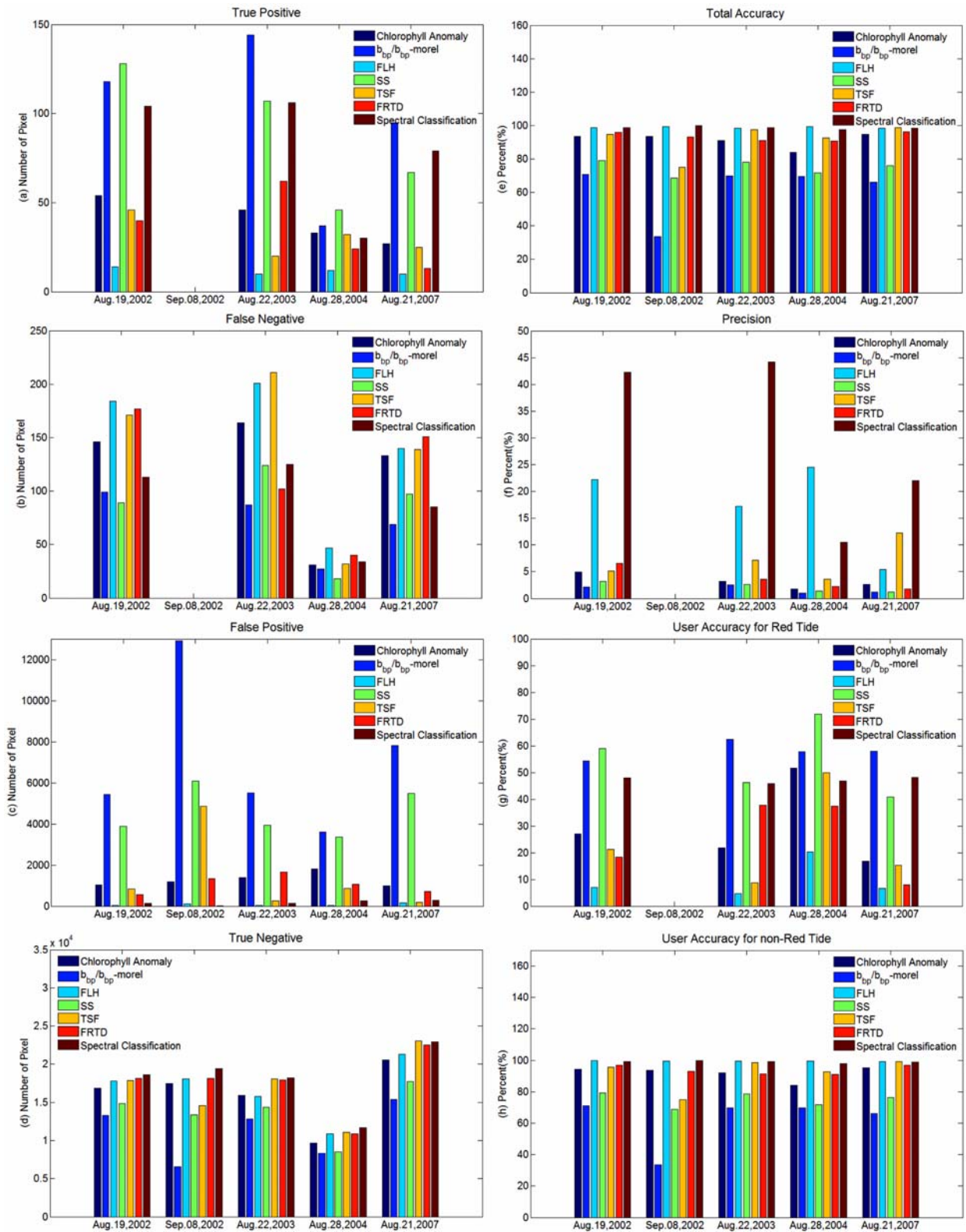
Fig. 17. Estimate for each detection and the accuracy of seven different red tide detection algorithms. The plots (left) show the pixel numbers for (a) true positive, (b) false negative, (c) false positive, (d) and true negative. The error assessment (right) was plotted by (e) total accuracy and (f) precision user accuracy for red tide (g) and non-red tide (h). All methods and statistics are shown in Tables 1 and 3

(Fig. 16e) appeared as a green or red color, with enhanced chlorophyll a concentrations (>5 mg/m^3), FLL (>0.05 mw/cm^2/μm/sr), and phytoplankton absorption (>0.1 1/m; Fig. 16a-d). The bright brown color in the area between Busan and Geoje-do corresponded to enhanced chlorophyll a concentrations (>10 mg/m^3) and phytoplankton absorption (>0.3 1/m). After applying the spectral classification (Fig. 10), the area of potential red tide was narrowed to within the red tide "alert" area between Sori-do and Geoje-do. Offshore waters contained small patches of potential red tide (Fig. 16f). On August 21, 2007 (Table 3), user accuracy for *C. polykrikoides* bloom and non-red tide using spectral classification was estimated to be 48.17% and 98.79%. A 48% of the *C. polykrikoides* bloom was flagged (true positive, 79 pixels) but 52% of that masked out (false negative, 85 pixels). In total, 280 pixels (false positive) were over-estimated as a *C. polykrikoides* bloom (precision of 22.01%).

Image analysis using proposed red-tide detection methods

Table 3 and Fig. 17 show the detection (number of pixel) and accuracy (%) as a function of each event that were used to calculate a relationship between the satellite and reference data (Table 2). The method for six different red tide detection algorithms is summarized in Table 1.

Although chlorophyll anomaly, FLH, TSF, and FRD methods were in fair agreement with high total accuracy and user accuracy of non-red tides, the precision and user accuracy of *C. polykrikoides* were relatively lower. This discrepancy resulted from increased detection of false negative and/or false positive areas compared to true positive areas. However, b$_{bp}$/b$_{bp}$_morel and SS algorithms showed relatively lower total accuracy, precision, and user accuracy for non-red tides but higher user accuracy for *C. polykrikoides*. Both, b$_{bp}$/b$_{bp}$_morel and SS methods, were related to increasing detection of false positive areas. In this study, the best estimates for detecting *C. polykrikoides* blooms were achieved with spectral classification. Notably, the accuracy assessment was not significantly different when determined using total accuracy, precision, or user accuracy for *C. polykrikoides* and non-red tides.

Maps of *C. polykrikoides* blooms (Figs. 12f-16f) in SSK were created using spectral classification (Fig. 10) and ocean color data were collected by MODIS. In the most notable difference was determined on events of September 8, 2002. The most onshore and offshore where high chlorophyll, FLH, and a_{ph}(443) (Fig. 13b-d) presented raised. The

contribution of gelbstoff/detritus absorption was higher compared to that of phytoplankton absorption in SSK and was associated with the presence of large amounts of non-pigment particulate or dissolved material that were inaccurately estimated as high satellite-derived chlorophyll concentrations (Ahn and Shanmugam 2006). Most red tide detection algorithms (chlorophyll anomaly, b$_{bp}$/b$_{bp}$_morel, SS, TSF, FRTD) estimated a large number of false positive areas and considered false satellite high chlorophyll water to be a *C. polykrikoides* bloom, whereas our analysis (spectral classification) dramatically reduced the false signal rate (false positive) from strong absorption at shorter wavelengths due to a large quantity of gelbstoff and detritus (Fig. 17, Table 3).

A second notable difference is the consistent user accuracy for *C. polykrikoides* blooms and non-red tides compared to that of the six different red tide detection algorithms. During each event, *C. polykrikoides* blooms were detected within ~50% using spectral classification, whereas TSF and FRTD, developed for detecting *C. polykrikoides*, provided coarse accuracy as they identified a small number of true positives and s large number of false positives. Retrieval of red tide data detected from satellites becomes even more difficult in waters where the signal from a small *C. polykrikoides* bloom is masked by the signal from a large quantity of inorganic particles or CDOM. Simple band ratios, included in both algorithms are not useful to distinguish CDOM from detritus in optically complex water and were identified as noise for our purpose.

5. Conclusions

With the aim of studying surface *C. polykrikoides* blooms in the optically complex SSK, we tested several simple approaches to discriminate red tide water from non-red tide water based on MODIS satellite-derived multi-spectral radiance, chlorophyll a, FLH, and IOPs (e.g., absorption and backscattering). The analysis demonstrated that radiance was strongly dependent on phytoplankton, CDOM, and suspended matter. The radiance peak shifted from violet-blue wavelengths to green wavelengths with increasing concentrations of organic and inorganic mater. Based on this spectral response and the results of previous studies, red tides were classified using four steps that were tested and applied to five different MODIS images. In steps 1 and 2 of the classification scheme, optically contrasting spectral

features are detected in the potential red tide, including a lower contribution of CDOM to chlorophyll, under clear water conditions, and a higher contribution of CDOM to chlorophyll in optically complex conditions in inshore areas. Different types of potential red tide waters are discriminated based on radiance spectra in steps 3 and 4.

Increased phytoplankton absorption at 443 nm and pigment backscattering at 555 nm resulted in a lower slope between 412 and 488 nm and a higher slope between 488 and 555 nm, which was linked by a hinge point at 488 nm. This result represents the spectral response of red tide water. The broader radiance spectra between the blue and green bands were associated with reduced pigment absorption and backscattering, and represented the spectral response of non-red tide water. Moreover, red tide water showed higher FLH values than did non-red tide water.

The analysis of MODIS ocean color imagery that captured *C. polykrikoides* blooms clearly showed discolored waters with enhanced pigment concentrations. The use of a pixel-based red tide classification, projected into distinct clusters in the space domain, revealed that red tide waters can be simply identified using several spectral bands of ocean color data. The accuracy of six different red tide detection methods and spectral classification was estimated and compared to validate our analysis. Our analysis, spectral classification, was more reliable and sensitive for detecting *C. polykrikoides* or non-red tide blooms than other red tide detection methods. This approach shows promise for regional mapping of phytoplankton blooms under various water conditions based on remote sensing data, because this method simply reproduces the spatial distribution of water types in the SSK. This approach is particularly important for interpreting dynamic coastal waters such as those in the SSK.

Acknowledgments

Reference

Ahn Y-H, Moon J-E (1998) Specific absorption coefficients for chlorophyll and suspended sediment in the Yellow and Mediterranean Sea. Korean J Remote Sens **14**(4):353-365

Ahn YH, Shanmugam P (2006) Detecting the red tide algal bloom from satellite ocean color observations in optically complex Northeast-Asia Coastal waters. Remote Sens Environ **103**:419-437

Ahn YH, Shanmugam P, Ryu JH, Jeong JC (2006) Satellite detection of harmful algal bloom occurrences in Korean waters. Harmful Algae **5**:213-231

Babin M, Morel A, Gentili B (1996) Remote sensing of sea surface sun-induced chlorophyll-a fluorescence: Consequences of natural variation in the optical characteristics of phytoplankton and the quantum yield of chlorophyll a fluorescence. Int J Remote Sens **17**:2417-2448

Bricaud A, Babin M, Morel A, Claustre H (1995) Variability in the chlorophyll-specific absorption coefficients of natural phytoplankton: analysis and parameterization. J Geophys Res **100**:13,321-13,332

Cannizzaro JP, Carder KL, Chen FR, Heil CA, Vargo GA (2008) A novel technique for detection of the toxic dinoflagellate, K. brevis, in the Gulf of Mexico from remotely sensed ocean color data. Cont Shelf Res **28**:137-158

Carder KL, Chen FR, Lee ZP, Hawes SK, Kamykowski D (1999) Semianalytic Moderate-Resolution Imaging Spectrometer algorithms for chlorophyll-a and absorption with bio-optical domains based on nitrate-depletion temperatures. J Geophys Res **104**:5403-5421

Ciotti AM, Lewis MR, Cullen JJ (2002) Assessment of the relationships between dominant cell size in natural phytoplankton communities and the spectral shape of the absorption coefficient. Limnol Oceanogr **47**(62):404-417

Dierssen HM, Kudela RM, Ryan JP, Zimmerman RC (2006) Red and black tides: Quantitative analysis of water-leaving radiance and perceived color for phytoplankton, colored dissolved organic matter, and suspended sediments. Limnol Oceanogr **51**(6):2646-2659

Esaias W, Abbott M, Barton I, Brown OB, Campbell JW, Carder KL, Clark DK, Evans RH, Hoge FE, Gordon HR, Balch WM, Letelier R, Minnett PJ (1998): an overview of MODIS capabilities for ocean science observations. IEEE Trans Geosci Remote Sens **36**:1250-1265

Franz BA (2006a) Extension of MODIS Ocean Processing Capabilities to Include the 250 & 500-meter Land/Cloud

Bands, NASA Ocean Biology Processing Group, Ocean Color Web. http://oceancolor.gsfc.nasa.gov/DOCS/modis_hires/

Franz BA (2006b) MSL12:The Multi-Sensor Level-1 to Level 2 Code, NASA Ocean Biology Processing Group, Ocean Color Web. http://oceancolor.gsfc.nasa.gov/DOCS/MSL12/

Gordon HR, Wang M (1994) Retrieval of water-leaving radiance and aerosol optical thickness over the oceans with SeaWiFS: a preliminary algorithm. Appl Optics **33**:443-452

Hooker SB, Firestone ER, Acker JC (1994) SeaWiFS Pre-launch Radiometric Calibration and Spectral Characterization. SeaWiFS technical report series, NASA Technical Memorandum 104566, Vol. 23

Hu C, Muller-Karger FE, Biggs DC, Carder KL, Nababan B, Dadeau D, Vanderbloemen J (2003) Comparison of ship and satellite bio-optical measurements on the continental margin of the NE Gulf of Mexico. Int J Remote Sens **24**(13):2597-2612

Hu C, Muller-Karger FE, Vargo GA, Neely MB, Johns E (2004) Linkages between coastal runoff and the Florida Keys ecosystem: a study of a dark plume event. Geophys Res Lett **31**. doi:10.1029/2004GL020382

Hu C, Muller-Karger FE, Taylor C, Carder KL, Kelble C, Johns E, Heil CA (2005) Red tide detection and tracing using MODIS fluorescence data: a regional example in SW Florida coastal waters. Remote Sens Environ **97**:311-321

IOCCG (2000) Remote sensing of ocean colour in coastal, and other optically-complex, waters. In: Sathyendranath S (ed) Report of the International Ocean-Color Coordination Group, no. 3, Dartmouth, 140 p

Ishizaka J, Kitaura Y, Touke Y, Sasaki H, Tanaka A, Murakami H, Suzuki T, Matsuoka K, Nakata H (2006) Satellite detection of red tide in Ariake Sound, 1998-2001. J Oceanogr **62**:37-45

Kang YS, Kim HG, Lim WE, Lee CK (2002) An unusual coastal environment and *Cochlodinium polykrikoides* blooms in 1995 in the South Sea of Korea. J Korean Soc Oceanogr **37**(4):1-12

Kim HG, Choi WJ, Jung YG, Park PS, An KH, Baek CI (1999) Initiation of *Cochlodinium polykrikoides* blooms and its environmental characteristics around the Narodo Island in the western part of South Sea of Korea. Bull Natl Fish Res Dev Inst Korea **57**:119-129 (in Korean)

Kim Y, Byun Y, Kim Y, Eo Y (2009) Detection of *Cochlodinium polykrikoides* red tide based on two-stage filtering using MODIS data. Desalination **249**:1171-1179

Lee D-K, Niller P (2003) Ocean response to Typhoon Rusa in the South Sea of Korea and in the East China Sea. J Korean Soc Oceanogr **38**(2):60-67

Lee D-K (2008) *Cochlodinium polykriklides* blooms and eco-physical conditions in the South Sea of Korea. Harmful Algae **7**:318-323

Lee SG, Kim HG, Bae HM, Kang YS, Jeong CS, Lee CK, Kim SY, Kim CS, Lim WA, Cho US (2002) Handbook of harmful marine algal blooms in Korean waters. National Fisheries Research and Development Institute, Republic of Korea, 172 p

Lee YS (2006) Factors affecting outbreaks of high-density *Cochlodinium polykrikoides* red tides in the coastal seawaters around Yeosu and Tongyeong, Korea. Mar Pollut Bull **52**:1249-1259

Letelier RM, Abbott MR (1996) An analysis of chlorophyll fluorescence algorithms for the Moderate Resolution Imaging Spectrometer (MODIS). Remote Sens Environ **58**:215-223

Lim WA, Lee YS, Lee SG (2008) Characteristic of environmental factors related to outbreak and decline of *Cochlodinium polykrikoides* bloom in the southeast coastal waters of Korea, 2007. J Korean Soc Oceanogr **13**(3):325-332 (in Korean)

McClain CR, Feldman GC, Hooker SB (2004) An overview of the SeaWiFS project and strategies for producing a climate research quality global ocean bio-optical time series. Deep-Sea Res II **51**:5-42

Morel A (1988) Optical modeling of the upper ocean in relation to its biogenous matter content (case I water). J Geophys Res **93**:10749-10768

Morel A, Maritorena S (2001) Bio-optical properties of oceanic waters: a reappraisal. J Geophys Res **106**:7163-7180

NFRDI (2004) Harmful Algal Blooms in Korean Coastal Waters from 2002 to 2003. National Fisheries Research and Development Institute, Republic of Korea, 274 p (in Korean)

NFRDI (2005) Harmful Algal Blooms in Korean Coastal Waters in 2004. National Fisheries Research and Development Institute, Republic of Korea, 95 p (in Korean)

O'Reilly JE, Maritorena S, Siegel DA, O'Brien MC, Toole D, Mitchell BG, Kahru M, Chavez FP, Strutton P, Cota GF, Hooker SB, McClain CR, Carder KL, Muller-Karger F, Harding L, Magnuson A, Phinney D, Moore GF, Aiken J, Arrigo KR, Letelier R, Culver M (2000) Ocean Color chlorophyll *a* algorithms for SeaWiFS, OC2 and OC4: Version 4. In: Hooker SB, Firestone ER (eds) *SeaWiFS Postlaunch Calibration and Validation Analysis, Part 3, SeaWiFS Postlaunch Tech. Rep. Ser.,* vol. 11, *NASA/TM-2000-206892*, NASA, Greenbelt, MD, pp 9-27

Ryan JP, Dierssen HM, Kudela RM, Scholin CA, Johnson KS, Sullivan JM, Fisher AM, Rienecker EV, Mcenaney PR, Chavez FP (2005) Coastal ocean physics and red tides : an example from Monterey Bay, California. Oceanogr **18**(2):246-255

Sasaki H, Tanaka A, Iwataki M, Touke Y, Siswanto E, Knee TC, Ishizaka J (2008) Optical Properties of Red Tide in Isahaya Bay, Southwestern Japan: influence of chlorophyll *a* concentration. J Oceanogr **64**:511-523

Sathyendranath S, Cota G, Stuart V, Maass M, Platt T (2001)

Remote sensing of phytoplankton pigments: a comparison of empirical and theoretical approaches. Int J Remote Sens **22**:249-273

Schofield O, Gryzmski J, Bissett WP, Kirkpatrick GJ, Millie DF, Moline M, Roesler CS (1999) Optical monitoring and forecasting systems for harmful algal bloom: possibility or pipe dream ? J Phycol **35**:1477-1496

Shanmugam P, Ahn Y-H, Ram PS (2008) SeaWiFS sensing of hazardous algal blooms and their underlying mechanisms in shelf-slope waters of the Northwest Pacific during summer. Remote Sens Environ **112**:3248-3270

Siegel DA, Maritorena S, Nelson NB, Behrenfeld MJ (2005) Independence and interdependencies among global ocean color properties: reassessing the bio-optical assumption. J Geophys Res **110**:C07011. doi:10.1029/2004JC002527

Stramski D, Kiefer DA (1991) Light scattering by microorganisms in the open ocean. Progr Oceanogr **28**:343-393

Stumpf RP, Culver ME, Tester PA, Tomlinson M, Kirkpatrick GJ, Pederson BA, Truby E, Ransibrahmanakuf V, Soracco M (2003) Monitoring Karenia brevis blooms in the Gulf of Mexico using satellite ocean color imagery and other data. Harmful Algae **2**:147-160

Suh YS, Jang LH, Lee NK, Ishizaka J (2004) Feasibility of red tide detection around Korea waters using satellite remote sensing. J Fish Sci Tech **7**(3):148-162

Tomlinson MC, Stumpf RP, Ransibrahmanakul V, Turby EW, Kirkpatrick GJ, Perderson BA, Gabriel AV, Heil CA (2004) Evaluation of the use of SeaWiFS imagery for detecting *Karenia brevia* harmful algal blooms in the eastern Gulf of Mexico. Remote Sens Environ **91**:293-303

Tomlinson MC, Wynne TT, Stumpf RP (2009) An evaluation of remote sensing techniques for enhanced detection of the toxic dinoflagellate, *Karenia brevis*. Remote Sens Environ **113**:589-609

Werdell PJ, Bailey SW (2005) An improved in-situ bio optical data set of ocean color algorithm development and satellite data product validation. Remote Sens Environ **98**:122-140

Wynne TT, Stumpf RP, Tomlinson MC, Warner RA, Tester PA, Dyble J, Fahnenstiel GL (2008) Relating spectral shape to cyanobacterial blooms in the Laurentian Great Lake. Int J Remote Sens **29**:3665-3672

Yoo S-J, Jeong J-C (1999) Detecting red tides in turbid waters. Korean J Remote Sens **15**(4):321-327